AGU PUBLICATIONS

Tectonics

RESEARCH ARTICLE
10.1002/2017TC004777

Key Points:
- We determined the stratigraphy and tectonic subsidence and uplift history of the western Musandam peninsula
- The tectonic subsidence and uplift indicate an initial age of rifting of 260 Ma and a final age of rifting of 185 Ma
- Tectonic subsidence indicates two compressional events that commenced at ~94 Ma and ~25 Ma, respectively

Correspondence to:
M. Y. Ali,
mali@pi.ac.ae

Citation:
Ali, M. Y., Aidarbayev, S., Searle, M. P., & Watts, A. B. (2018). Subsidence history and seismic stratigraphy of the western Musandam peninsula, Oman–United Arab Emirates mountains. *Tectonics*, *37*, 154–181. https://doi.org/10.1002/2017TC004777

Received 23 AUG 2017
Accepted 25 OCT 2017
Accepted article online 15 DEC 2017
Published online 17 JAN 2018

Subsidence History and Seismic Stratigraphy of the Western Musandam Peninsula, Oman–United Arab Emirates Mountains

M. Y. Ali[1], S. Aidarbayev[2], M. P. Searle[3], and A. B. Watts[3]

[1]The Petroleum Institute, Abu Dhabi, United Arab Emirates, [2]ADNOC, Abu Dhabi, United Arab Emirates, [3]Department of Earth Sciences, Oxford University, Oxford, UK

Abstract Seismic reflection profiles, exploratory well, and outcrop data are used to determine the stratigraphy and tectonic subsidence and uplift history of the western Musandam peninsula. Five major regional megasequences have been recognized: (1) Permian to Late Cretaceous rifted margin sequence, (2) Late Cretaceous Aruma foreland basin sequence that evolved in response to the obduction of the Semail Ophiolite, (3) early–mid-Cenozoic Pabdeh foreland basin sequence that formed due to orogenic loading associated with the early continent–continent collision of the Arabian and Eurasian plates in the Zagros mountains of central Iran, (4) a sequence above the mid-Miocene unconformity that marks the final stage of continent–continent collision, and (5) a sequence above the late Pliocene unconformity interpreted as tilting due to the latest stage of continent–continent collision. In addition, seismic and outcrop data captured multiple west-verging and east-dipping thrust faults associated with the deformation of the Hagab thrust, which causes repetition of the Permian–Mesozoic shelf sequence and the early–mid Cenozoic foreland basin sequence. The tectonic subsidence and uplift derived from backstripping can be explained by a model in which the margin developed by uniform depth extension with an initial age of rifting of 260 Ma and a final age of rifting of 185 Ma. Moreover, the tectonic subsidence indicates two compressional events that commenced at ~94 Ma and ~25 Ma, respectively. These events are attributed to the obduction of the Semail Ophiolite and the culmination of the Musandam peninsula, respectively.

1. Introduction

The Musandam peninsula at the northern end of the Oman–United Arab Emirates (UAE) mountains marks the transition between the Late Cretaceous Tethyan ocean–continent collision and the late Cenozoic continent–continent collision (Searle, 1988b; Searle et al., 2014). These collisions led to an evolution of the Late Cretaceous Aruma basin and the late Cenozoic Zagros foreland basin, respectively, with a transitional early–mid-Cenozoic Pabdeh foreland basin in between as a result of the Musandam culmination.

The Musandam peninsula records a passive margin sequence of Permian to Cenomanian age (Glennie et al., 1974; Hudson et al., 1954; Ricateau & Riche, 1980). Hudson et al. (1954) were the first to describe the stratigraphy and structure of the area. They recognized Permian to Lower Cretaceous strata that was dominated by limestone and has a total thickness of 3,408 m, as well as several hundred meters of Jurassic and Lower Cretaceous tuffs and radiolarian cherts. Maurer et al. (2008) provided a reconstruction of the Late Permian and Triassic depositional history of the Wadi Bih area based on facies analysis and foraminiferal biostratigraphy. Al-Suwaidi et al. (2016) studied the Ghalilah Formation in Wadi Milaha, which provides a complete equatorial shallow water carbonate sequence through the Upper Triassic to Lower Jurassic interval. Furthermore, Philips (2013) provided Jurassic–Cretaceous stratigraphical and palaeogeographical reconstruction of the southern margin of Neotethys based on geological mapping of the UAE undertaken by the British Geological Survey (Styles et al., 2006).

However, there have been few quantitative studies of subsidence and uplift history of the Musandam peninsula, due to the lack of subsurface data and the deformed nature of the exposed strata. Nevertheless, understanding the structural configuration of the Musandam peninsula is of great interest in order to understand the early stages of a continental collision and the subsurface structure and to target potential oil and gas structural traps.

The aim of this paper is to use exploratory wells, seismic reflection profiles, and surface geology to determine the tectonic subsidence and uplift history of the western Musandam peninsula. By backstripping the data, we have determined the tectonic subsidence and uplift history and used it to constrain the rifting history of the region. We show that the western Musandam peninsula has been subjected to two main rifting events and two compressional events, which have resulted in the development of Aruma and Pabdeh foreland basins, respectively.

2. Geological Setting

The western Musandam peninsula is located at the northeastern edge of the Arabian plate (Figure 1). Early stages of the Arabian plate amalgamation started from the Neoproterozoic compressional tectonics (from ca. 715 to 610 Ma) of the island-arc and microcontinental portions accreted against the Gondwana supercontinent with N–S trending structures (inset of Figure 1; Al-Husseini, 2000). These trends appear throughout the UAE, but they are particularly well defined toward the west by Bouguer gravity anomalies (Ali et al., 2014). Intracratonic sag basins evolved during the Neoproterozoic–Late Devonian period (~610 to 364 Ma) when the Arabian plate was located within the continental interior of Gondwana (Sharland et al., 2001). This tectonic setting was inherited by the NW–SE trending Najd strike-slip fault system and is manifested by the well-defined Abu Dhabi Lineament in the central UAE (Ali et al., 2014). Regionally thick Ediacarian–Early Cambrian salt basins, Ara and Hormuz, persisted in most of the Oman and UAE region. The Ara salt basin has a NE trend and is present across south-central Oman (Reuning et al., 2009). The Hormuz salt covers the north and northwestern part of the UAE where deep-seated bodies locally pierce the overlying sedimentary cover forming dome structures characterized by gravity anomaly lows (Ali et al., 2014). From Middle Cambrian to Devonian, the Arabian plate was located on a broad stable platform of the Gondwana rifted margin, which allowed deposition of mainly marine sandstone, shale, and minor carbonates (Faqira et al., 2009; Ruban et al., 2007; Sharland et al., 2001; Stampfli et al., 2001).

From the Late Devonian to the Early Carboniferous, the Arabian plate was affected by a major tectonic event with crustal-scale basin and arch structures, which reactivated the N–S trending Neoproterozoic basement faults and resulted in regional uplifts with widespread erosion or nondeposition (Faqira et al., 2009; Husseini, 1992; Konert et al., 2001; Ruban et al., 2007). This tectonic event is generally interpreted as a far-field stress related to the Hercynian orogeny, which resulted from the collision of Laurasia and Gondwana and the closure of the intervening Rheic Ocean (Al-Husseini, 2004; Johnson, 2008; Konert et al., 2001). However, recent studies based on outcrops and borehole correlations in the Iranian High Zagros Belt suggest this tectonic event is caused by diffuse extensional deformation and by thermal uplift caused by volcanism (Frizon de Lamotte et al., 2013; Tavakoli-Shirazi et al., 2013). Furthermore, xenoliths brought to the surface by Neogene volcanism in the northern Arabian plate yield U–Pb zircon ages of ~357 Ma (Early Carboniferous), which is interpreted to approximate when these magmas crystallized (Stern et al., 2014). This may support the notion of a major episode of thermal uplift in the Early Carboniferous. In agreement with this interpretation, Ali et al. (2017) mapped possible Late Paleozoic NW-trending volcanic/magmatic bodies in the central and northwestern UAE using aeromagnetic data.

During the Late Carboniferous–Early Permian, the Arabian plate was subjected to subsidence governed by the progressive cooling of the lithosphere allowing deposition of predominantly continental clastic sediments of the Unayzah Formation (Al-Husseini, 2004; Al-Laboun, 1987; Faqira et al., 2009; Frizon de Lamotte et al., 2013). From middle Permian to Late Cretaceous, the northeastern Arabian plate was a rifted margin of the Neo-Tethys Ocean (Ruban et al., 2007). High rates of subsidence created the accommodation space for the deposition of mainly thick carbonates of the Rus al Jibal, Elphinstone, Musandam, Thamama, and Wasia Groups (Searle et al., 2014; Figure 2). The Late Permian to Late Cretaceous shelf carbonate platform outcrops over a vast area of the Musandam peninsula (Glennie et al., 1974).

Rifted margin evolution was then interrupted by the obduction of the Semail Ophiolite during the Late Cretaceous (from the Late Cenomanian to the Early Maastrichtian; Searle, 1988a). The Semail Ophiolite thrust sheet is approximately 8–15 km thick and is composed of a harzburgite and dunite mantle and a gabbro-dyke-basaltic oceanic crustal sequence, which were formed above a NE-dipping subduction zone, prior to

Figure 1. Geological map of the Musandam peninsula in the northeastern Arabian plate. The map shows 17 exploration wells and six seismic profiles used in this study plus four deep seismic profiles acquired by WesternGeco (Tarapoanca et al., 2010). Inset represents location of the study area within structural and tectonic map of the Arabian plate, which shows regional lineaments and faults (Sharland et al., 2001). The white line shows location of Figure 8.

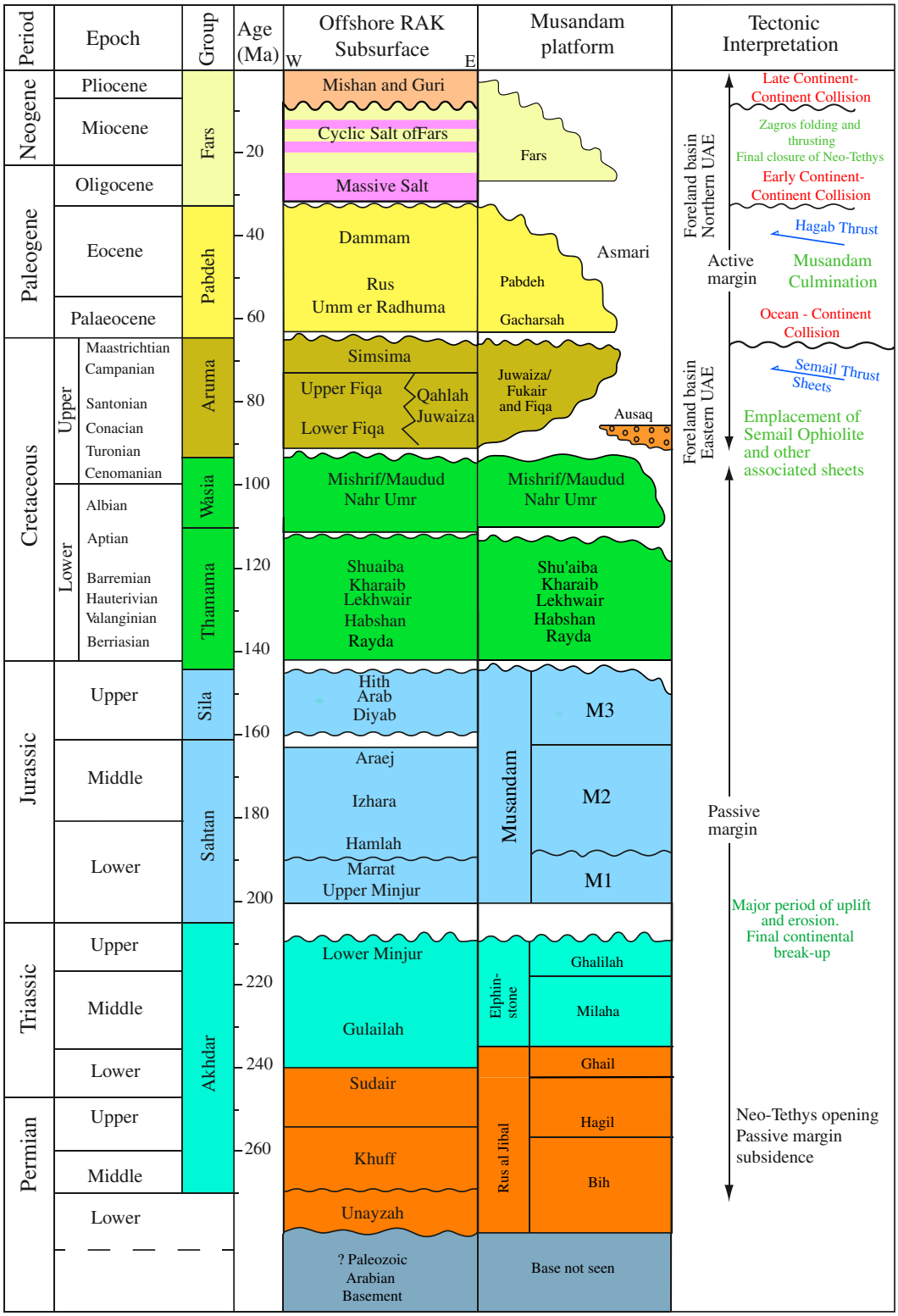

Figure 2. Summarized regional tectonostratigraphic chart, modified after Searle et al. (2014). Chart illustrates stratigraphic groups and formation names beneath the subsurface of Ras Al Khaimah and in the outcrop of the Musandam Platform.

obduction (Searle et al., 2015; Searle & Malpas, 1980). The obduction process loaded the surface of the Arabian plate causing flexure and formation of the Late Cretaceous Aruma foreland basin (Ali & Watts, 2009; Ali et al., 2013; Warburton et al., 1990).

The obduction of the Semail Ophiolite ended at ~70 Ma (Maastrichtian) and was followed by a stable period of shallow marine carbonate deposition (Searle, 2007). Carbonate deposition was interrupted in the late Oligocene–early Miocene as a result of continent–continent collision between the Arabian and Eurasian plates, which caused the Zagros fold belt and the Musandam culmination (Searle, 1988b).

3. Seismic Stratigraphy of the Rifted Margin and Overlying Foreland Basins

Six seismic lines and well data (Figure 3) were used to determine major structures and stratigraphic sequences, particularly the geometry of the Mesozoic rifted margin, Late Cretaceous Aruma foreland basin, early–mid-Cenozoic Pabdeh foreland basin, and the Hagab thrust on the western edge of the Musandam peninsula (Figure 1). Line 1 is 14 km in length and trends SE–NW in a direction perpendicular to the coastline (Figure 4). Figure 5 shows a seismic profile that consists of Lines 2 and 3. The profile is 43 km in length and runs subparallel to the coastline and to the strike of the Hagab thrust (Figure 1). Figure 6 shows a composite seismic profile that is 45 km in length, which is composed of Lines 4, 5, and 6. The profile trends to SE–NW and extends into both onshore and offshore areas.

The seismic profiles are confined to areas of narrow coastal plain and rough terrain along the mountain front and generally are of poor quality. It is therefore difficult to clearly image subsurface structures. Nevertheless, wells that are located at or close to the seismic profiles (Aman-1, Rahman-1, Jazirat Huwlaylah-1x, and Jiri-1x) were used to tie the seismic to the stratigraphy (Figure 3). Well logs and check-shot data were used to identify key reflections from the Permian to Neogene succession corresponding to unconformities and sequence boundaries. As a result, formation tops and laterally continuous reflectors allowed us to delineate five stratigraphic sequences that are regionally mappable. These are as follows: (1) Permian–Cretaceous shelf carbonates (Rus Al Jibal, Elphinstone, Musandam, Thamama, and Wasia Groups); (2) Late Cretaceous foreland sequence (Aruma Group); (3) early–mid-Cenozoic foreland sequence (Pabdeh Group); and (4) late Cenozoic (Fars Group) together with (5) deposits above the late Pliocene unconformity (Mishan and Guri Groups).

3.1. Permian–Cretaceous Shelf Carbonates

This stratigraphic megasequence represents the rift margin shelf carbonates and is subdivided into Permian, Triassic–Jurassic, and Cretaceous sequences. The Permian sequence is contaminated with multiples, and only the Jiri-1x well penetrates the sequence along the seismic profiles. Therefore, it was not possible to correlate the sequence across all the seismic profiles. Hence, we treated all the reflectivity below the Triassic–Jurassic shelf carbonates as representative of an undifferentiated Paleozoic sequence.

The Triassic–Jurassic sequence has only been sampled in the Jiri-1x well, which is located along Line 6 (Figure 6b). However, the Ghubbali-1, Bukha-2 (Figure 3a), and HD-1 (Figure 3b) and Hagil-1x, Sharjah-2, Peter-1, and Sajaa-1 wells (Figure 3c) penetrate the sequence, but they are not located on the seismic profiles. On Line 1 and Lines 4–6, the top of Jurassic shelf carbonate is picked from a lateral continuous reflector that exhibits low amplitude (Figures 4b and 5b). Internally, the succession has high-amplitude continuous and subparallel reflections. To the east, several structurally Hagab-associated imbricate thrusts emplace Triassic–Jurassic shelf carbonate onto Cretaceous sequence, and fault planes seem to extend to great depth where the Permian sequence is expected.

The Cretaceous sequence is composed of the Wasia and Thamama Groups (Figures 4b, 5b, and 6b). Most of the prolific oil reservoirs of the UAE and Oman are found within these groups (Alsharhan, 1989; Forbes et al., 2010). Therefore, almost all of the exploration wells penetrate the Wasia Group and the upper formations of the Thamama Group (Shuaiba, Kharaib, and Lekhwair Formations; Figure 3). The top of the sequence (top of the Wasia Group) is prominent with an erosional surface to the east (Figure 5b).

3.2. Late Cretaceous Foreland Basin Sequence (Aruma Group)

Deposits of the Aruma Group, which starts with onlap onto the erosional surface of the Wasia Group, mark the transition to a foreland basin that developed in front of the advancing thrust sheets of the Late

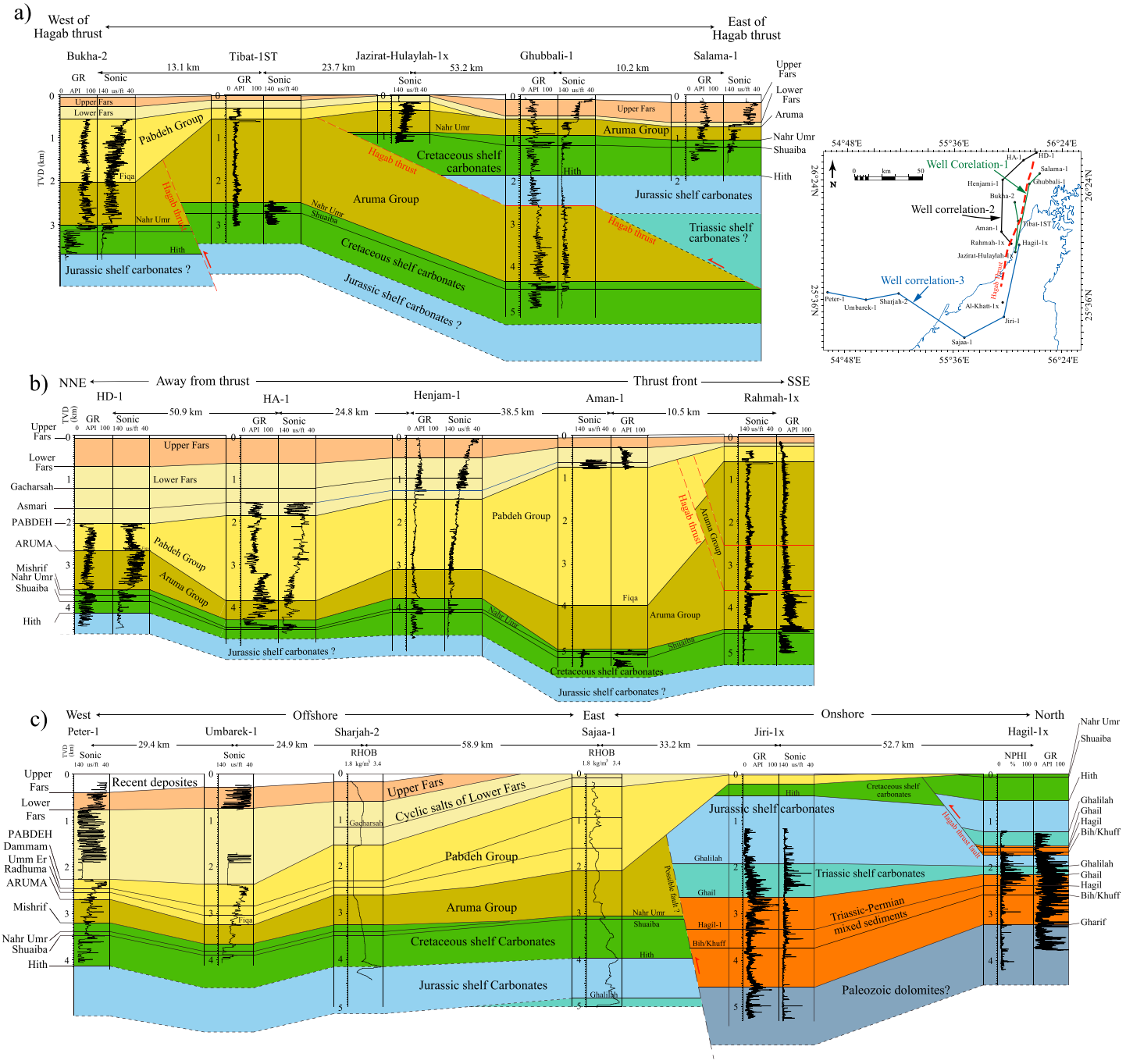

Figure 3. Major stratigraphic sequences regionally interpreted by correlation of exploration wells (refer to the inset on the top right for locations) where Sonic, GR, RHOB, and NPHI logs are used to qualitatively control the correlation. (a) Well correlation-1 shows the wells located at foot (west) and hanging walls (east) of the Hagab thrust, which captured repeated duplex stratigraphy. (b) Well correlation-2 starts from the wells next to the Hagab thrust front and extends away toward the Zagros Fold Belt to the north. The correlation shows stratigraphic repetition toward the east due to stacking caused by the Hagab thrust. (c) Well correlation-3 starts from the wells next to the Hagab thrust front, passes through the Dibba associated faults, and extends away toward the offshore Sharjah to the west. This well correlations document the deformation of subsurface layers by the Semail thrust that occurred during the Late Cretaceous.

Cretaceous Semail Ophiolite. The seismic profiles indicate that the basin thickens to the east forming a wedge-shaped geometry (Figure 4). However, it is difficult to interpret the upper boundary of the Aruma Group close to the Hagab thrust due to intense deformation that resulted in discontinuous reflectors.

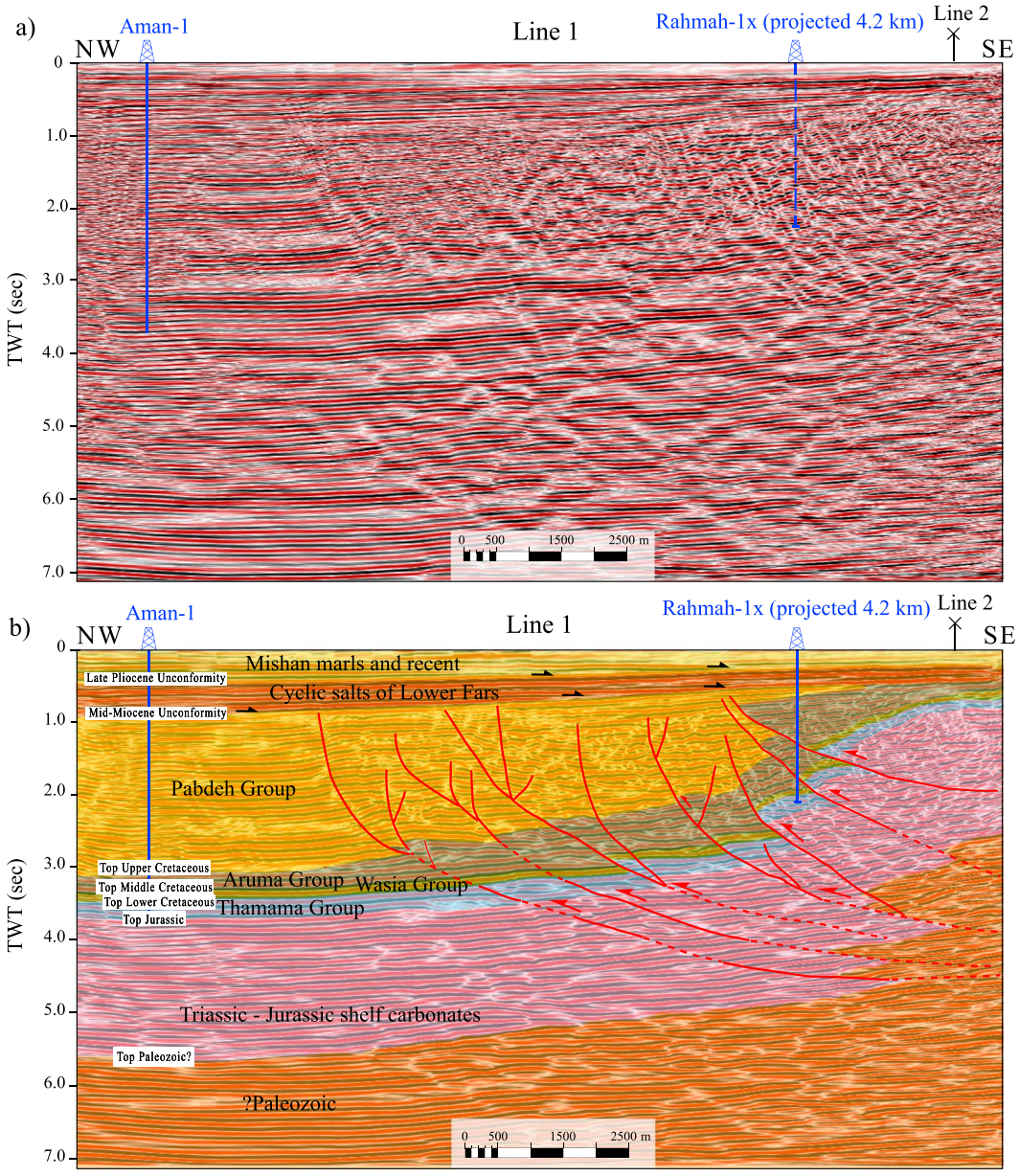

Figure 4. (a) Uninterpreted seismic profile of Line 1. (b) Interpreted seismic profile of Line 1. Aman-1 and Rahmah-1x wells were used to tie seismic and well data. The profile extends across the strike of the Musandam peninsula and shows compressional structural deformations to the southeast. The seismic section captures the thickest part of the Pabdeh foreland basin. Vertical exaggeration is ~1. See Figure 1 for location.

3.3. Early–Mid-Cenozoic Foreland Sequence (Pabdeh Group)

The base of the early–mid-Cenozoic sequence (Pabdeh Group) onlaps the erosional surface of the Aruma Group to the east, and the reflectors become more conformable away from the thrust front to the west (Figures 4b and 6b). The mid-Cenozoic compressional tectonic event is expressed as localized anticlines with no clear root or linkage to the Hagab thrust (Line 3 on Figure 5 and seismic Line 5 on Figure 6). Therefore, the syn-tectonic deposition of the Pabdeh Group is marked by onlapping reflectors on top of the flanks of anticlines, while the reflectors appear as downlap on the base of the synclines. The top of the Pabdeh Group is in an angular unconformity with the Fars Group over the anticlines; elsewhere, the group appears disconformable with overlying sequences (Figures 4b, 5b, and 6b).

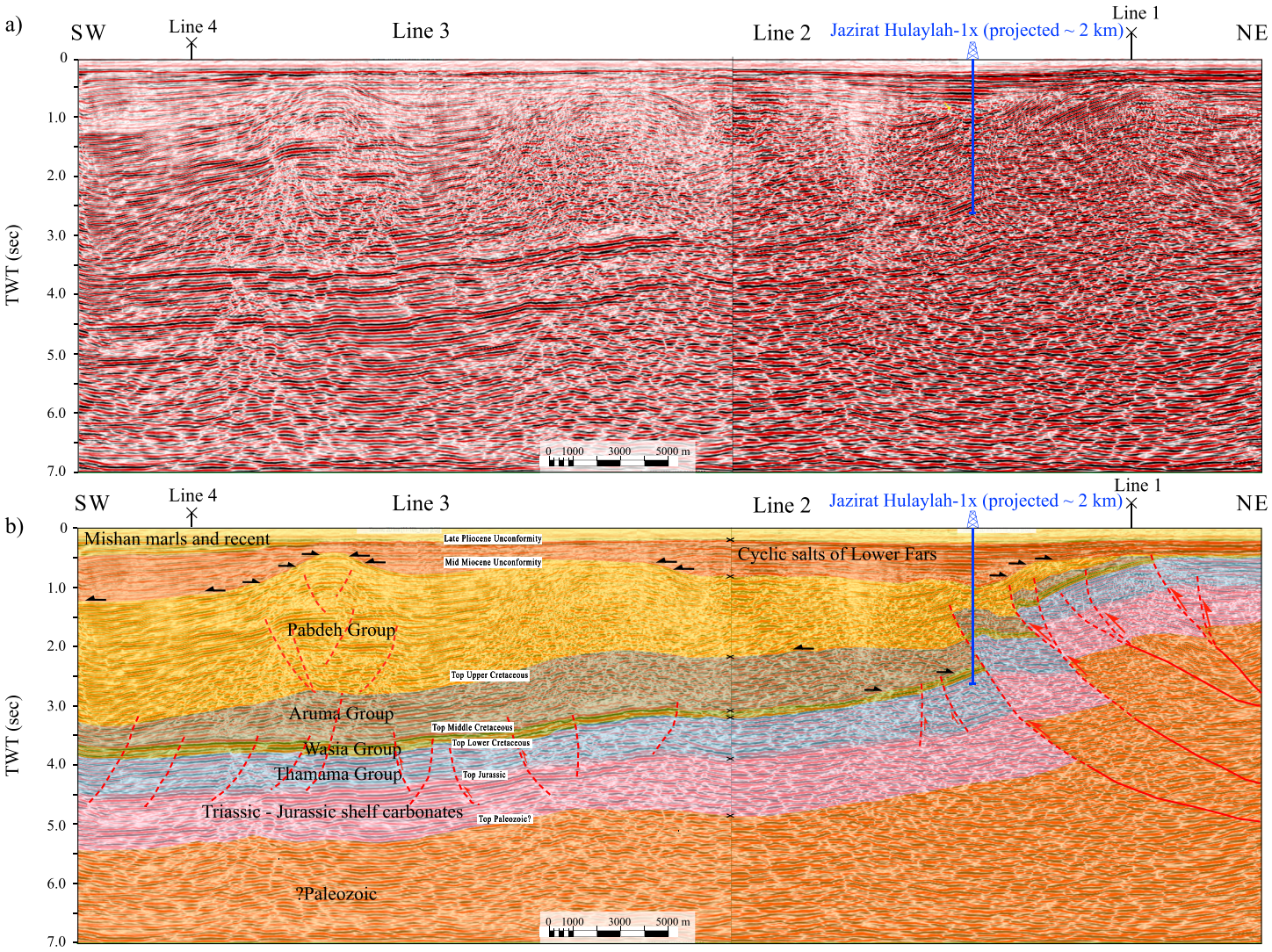

Figure 5. (a) Uninterpreted seismic profile of Lines 2 and 3. Jazirat-Hulaylah-1x well reached the Thamama Group at the northeastern end of the profile. (b) Interpreted seismic profile of Lines 2 and 3. The profile runs along the strike of the Musandam peninsula where the Aruma Group thickening toward the south and eroded in front of the Hagab thrust in the north. Black arrows indicate truncations and onlaps. Refer to Figure 1 for location of the seismic lines.

3.4. Late Cenozoic Sequence (Fars Group)

The Fars Group is deposited above the mid-Miocene unconformity with low-angle tilting and onlapping stratal patterns mainly to the east (Figures 4b, 5b, and 6b). The top of the group is bounded by the late Pliocene unconformity. The imbricate thrust faults associated with the Hagab thrust extend up to the surface at the eastern edge of Line 6 (Figure 6b) resulting in uplift and partial erosion of the sequence.

3.5. Late Pliocene Sequence (Mishan and Guri Formations)

The most recent sequence exhibits strong and continuous amplitudes at the base with onlaps on the low-angle late Pliocene unconformity. The internal reflectors weaken upward where their discontinuity become more dominant (Figures 4b, 5b, and 6b). The eastern edge of Line 6 is marked by erosion or nondeposition of the sequence due to reactivation of Hagab-associated imbricate thrust faults (Figure 6b).

4. Balanced and Restored Cross Sections

Known stratigraphic thicknesses both in the mountains and in three wells drilled in the Arabian Gulf, offshore Aman-1, offshore Rahmah-1x, and onshore Hagil-1x (Figures 3 and 7) were used to construct a balanced cross

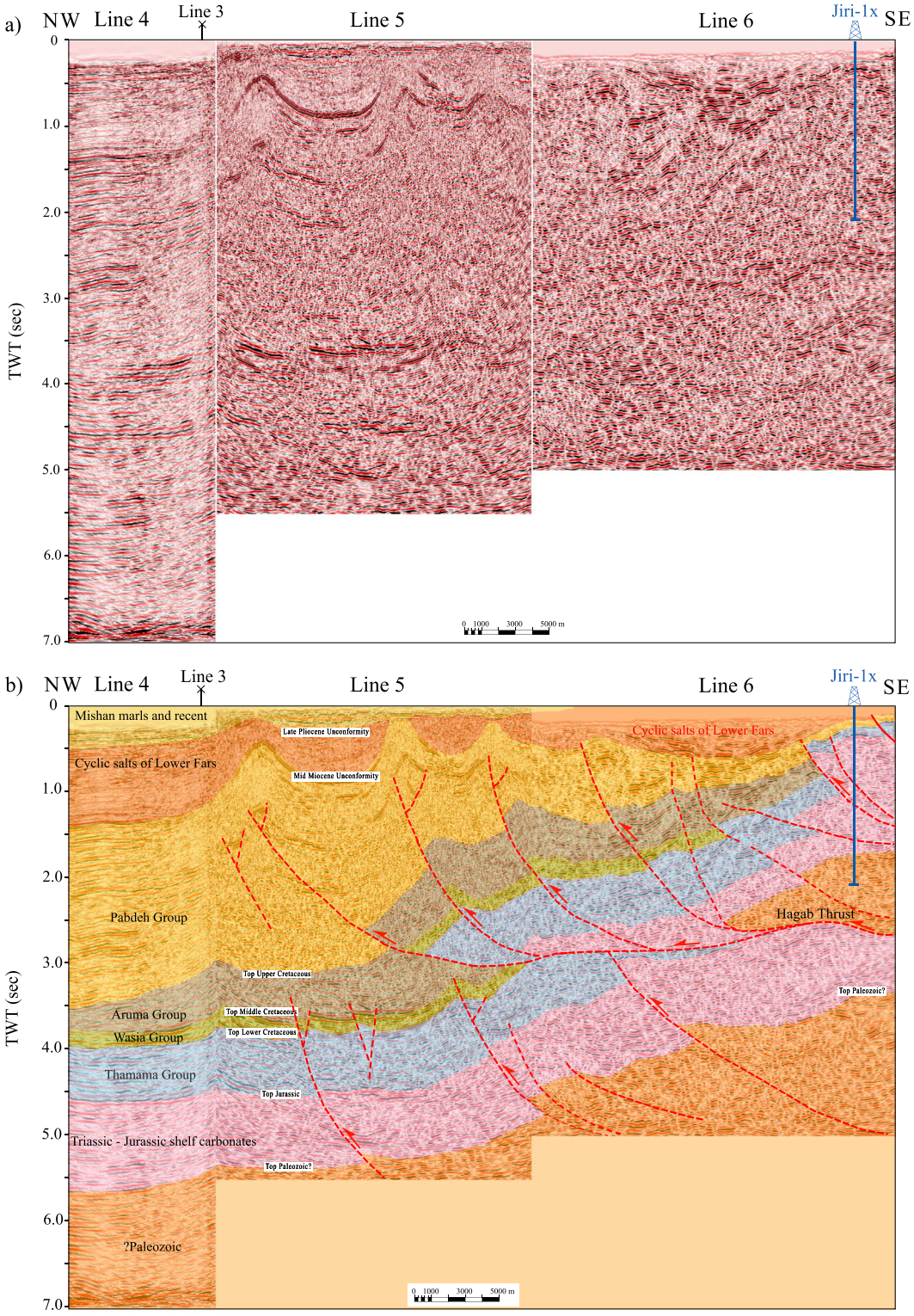

Figure 6. (a) Uninterpreted seismic profile of Lines 4, 5, and 6. (b) Interpreted seismic profile of Lines 4, 5, and 6. For location, see Figure 1.

section across the Musandam peninsula (Figure 8). The cross section is also constrained using available seismic profiles (see section 3). Figure 9 is a restored cross section showing the positions of each thrust sheet prior to thrusting. The thickness of the Pabdeh Group reaches 3,170 m in Aman-1 well, reducing to

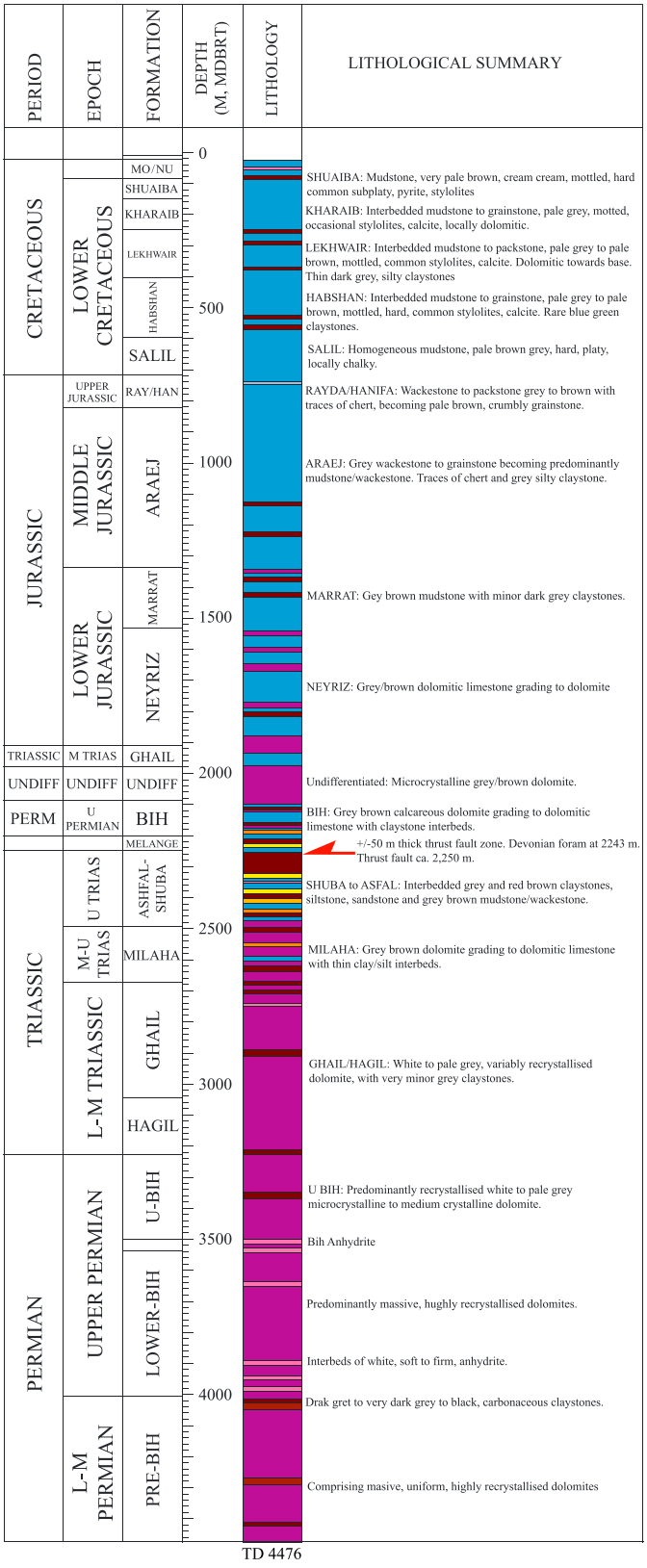

Figure 7. The stratigraphy penetrated by the Hagil-1x well, modifed from Indago-Petroleum (2006). MDBRT stands for Measured Depth Below Rotary Table.

only a few hundred meters in Rahmah-1x. Several steeply inclined thrusts including the Bukha thrust are extrapolated from the north. Offshore seismic and well data show that the Henjam-1 and Bukha-2 wells drilled through the foreland, whereas the Ghubbali-1 and Salama-1 wells drilled into the Hagab thrust hanging wall (Michaelis & Pauken, 1990; Ricateau & Riche, 1980; Searle et al., 1983, 2014). Thrust tip lines are truncated by the base of the Miocene Fars and Mishan Groups giving an upper time limit for Musandam thrusting (Figure 4). These thrusts have the effect of progressively raising the shelf carbonates to the east and reducing the thickness of the Pabdeh foreland basin fill toward the mountain front.

The most prominent Oligocene thrust is the Hagab thrust, which is exposed onshore in the Hagil Window in Ras Al Khaimah (Figure 10). The large front fold above the Hagab thrust emplaces the entire Permian–Mesozoic shelf sequence over a thin thrust sheet of Hawasina cherts and Haybi volcanic rocks exposed around the Hagil Window (Searle, 1988b; Searle et al., 2014). The Hagab thrust shows a minimum of 8 km westward transport emplacing pre-Permian basement rocks and Permian–Mesozoic shelf carbonates over the entire Permian–Mesozoic sequence as well as a thin overlying sheet of Hawasina–Haybi rocks. Three other thrusts to the east of the Hagab thrust have the effect of thickening and raising the shelf carbonates progressively to the east. The deepest exposed rocks in Musandam are Permian shelf carbonates exposed along the SE coast. These are cut by the large-scale ESE-dipping Dibba normal fault that has a throw of at least 5 km.

The eastern part of the cross section is extrapolated from the Dibba zone rocks to the south. The Dibba zone shows the full range of Upper Permian and Mesozoic shelf margin (Sumeini Group), proximal basin (Hamrat Duru Group) and distal Tethyan (Shamal cherts, Hawasina complex), and trench (Haybi thrust sheet) rocks emplaced toward the west in a series of thin-skinned thrust sheets (Searle, 1988a; Searle et al., 2014). The Semail Ophiolite forms the uppermost thrust sheet and extends offshore Dibba and the UAE.

5. Subsidence and Uplift History of the Western Musandam Peninsula

5.1. Data

Seventeen exploration wells located in the west of the Musandam peninsula were used in this study (Table 1 and Figure 1). The deepest well (Aman-1) was drilled to a depth of 5,396 m below sea level. However, the Hagil-1x, Jiri-1x, and Sajaa-1 wells penetrated the oldest stratigraphic formations.

Reference points of drilling depth in MD (measured depth) were adjusted to TVDSS (true vertical depth sub sea) below mean sea level using the RTKB (Rotary Table Kelly Bushing) elevation (KB plus ground level) in all wells, and major stratigraphic groups have been correlated between them (Figure 3). Sonic, gamma (GR), neutron porosity (NPHI), and density (RHOB) logs are extracted from wells and used for the well correlations. Sonic and GR are present almost in all wells, while Sajaa-1 and Sharjah-2 wells have RHOB logs only. The NPHI log exists only in reservoir intervals of recently drilled wells, Tibat-1ST and Hagil-1x.

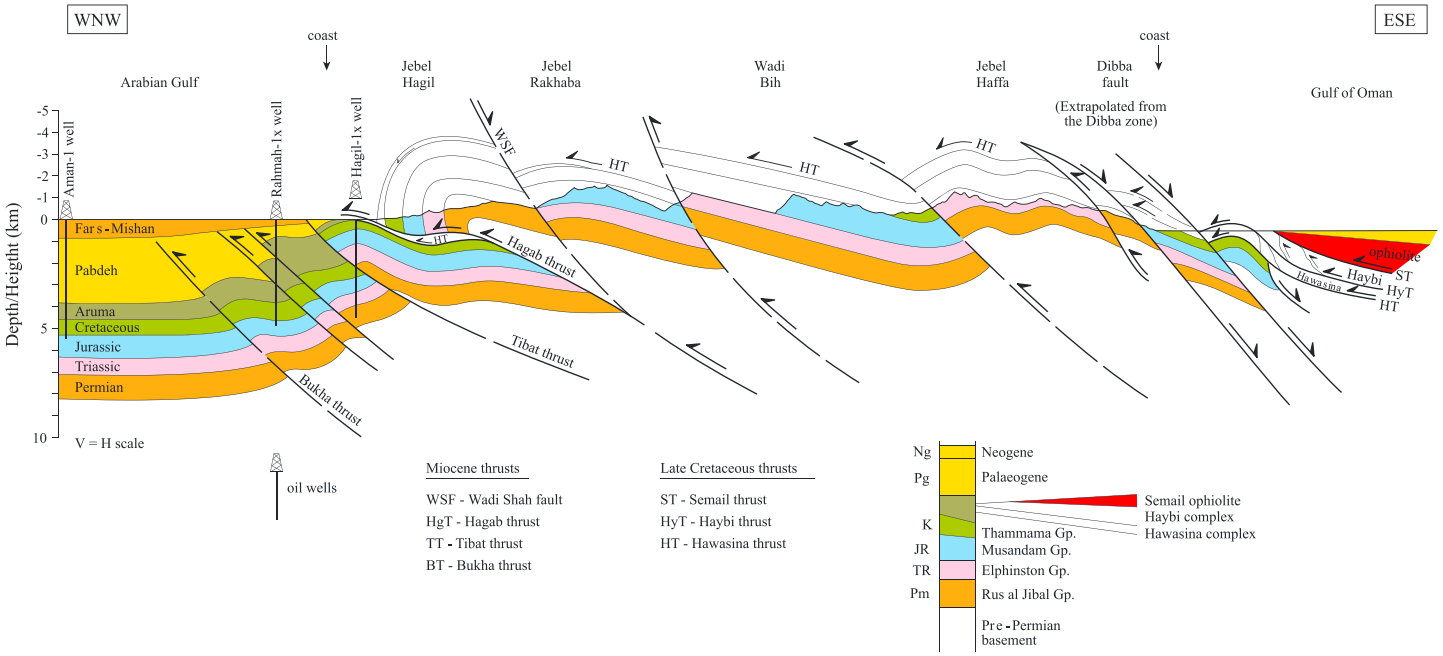

Figure 8. A cross-section across the Musandam peninsula balanced for the known stratigraphic thicknesses both in the mountains and in three wells drilled in the Arabian Gulf, offshore Aman-1, offshore Rahmah-1x, and onshore Hagil-1x. See Figure 1 for the location of section.

5.2. Backstripping

5.2.1. Biostratigraphic Data

A backstripping technique was used to quantitatively determine the depth that basement would have been in the absence of sediment and water loading (Watts & Ryan, 1976). This basement depth was then used to constrain the timing, duration, and the magnitude of the tectonic subsidence and uplift caused by other factors such as rifting and orogenic loading.

We first compiled the depth and ages of 41 formation tops ranging in age from 2.7 to 260 Ma (Table 2). The geological ages were determined from well reports where paleontological studies were used to identify the stratigraphic boundaries. However, Peter-1, Sharjah-2, and Umbarek-1 wells did not have well reports and had only stratigraphic formation names. We approximated the ages of these horizons using the International Stratigraphic Chart compiled by the International Commission on Stratigraphy (www.stratigraphy.org) and the geologic timescale (Gradstein et al., 2012).

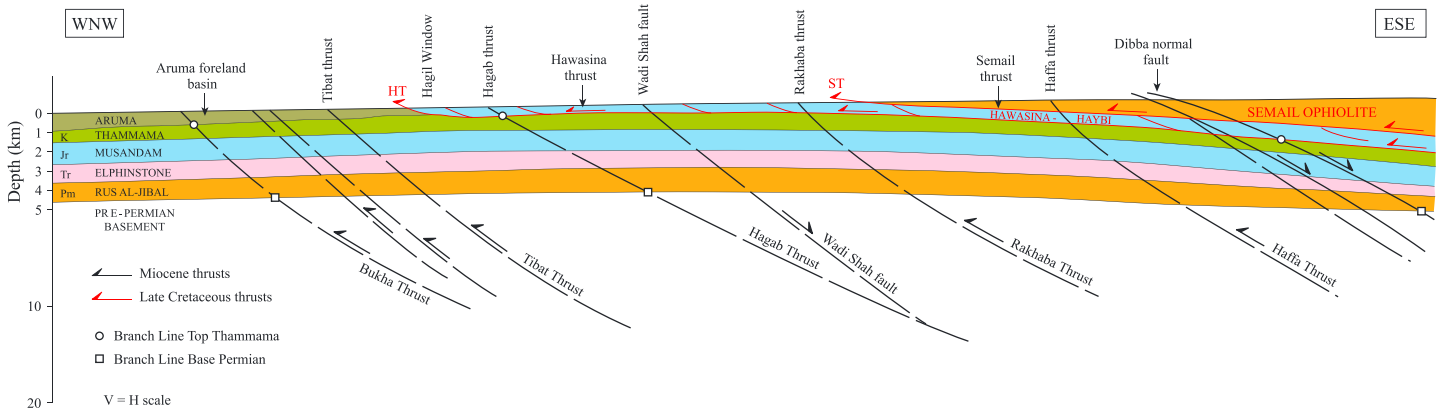

Figure 9. A restored section of the cross-section shown in Figure 8 showing the positions of each thrust sheet shown in Figure 8 prior to thrusting.

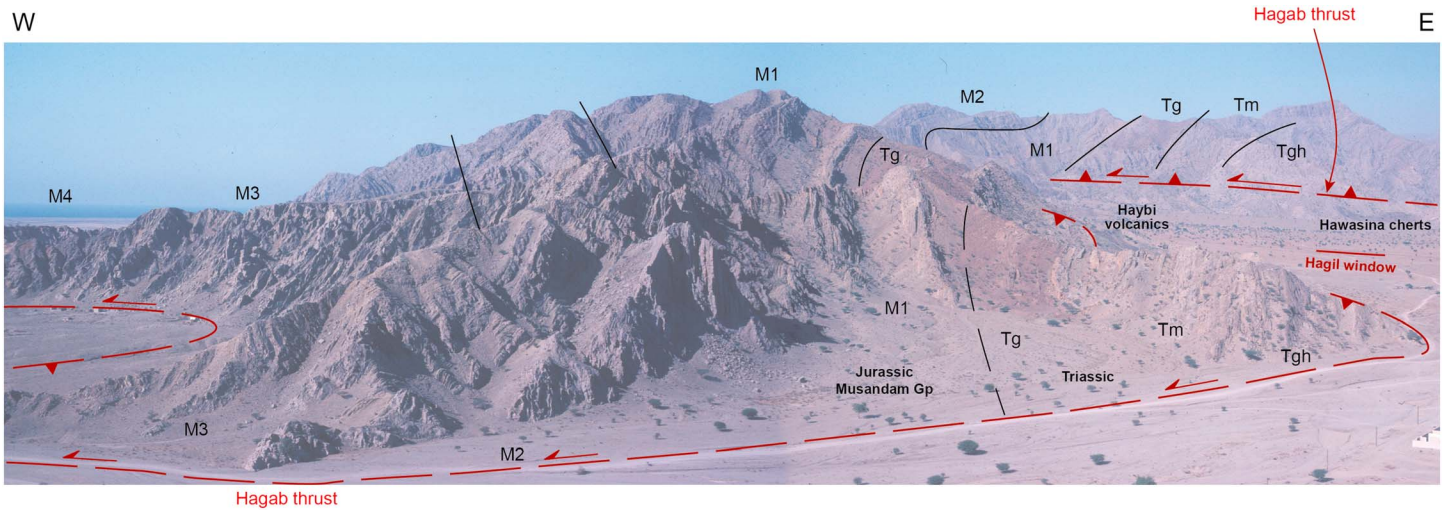

Figure 10. View to the north of the Hagab thrust in Hagab Window, Ras al Khaimah. Tg, Tm, and Tgh represent the Ghail, Milah, and Ghalilah Formations, respectively.

5.2.2. Decompacted Thickness of Sedimentary Layers

The thickness of sedimentary layers observed today differs from what it was in the past because of overburden pressure and chemical and mechanical compaction (Schneider et al., 1996). In this study, stratigraphic layers were progressively decompacted using empirically derived porosity versus depth curves and the methodology described by Steckler and Watts (1978). Present-day porosity values can be obtained from exploration well logs such as neutron porosity (NPHI) or sonic. Unfortunately, the well data show that the majority of neutron porosity measurements were acquired from reservoir zones. However, sonic logs are mostly available throughout the entire drilled sections of the 17 wells. The porosity can be calculated from the sonic logs using the modified equation of Wyllie (Wyllie et al., 1956) where the porosity varies with lithology (Raiga-Clemenceau et al., 1998).

5.2.3. Paleobathymetry

There are several sources of data that can be used to predict the paleobathymetry of a particular stratigraphic formation at the time of deposition. Results of biostratigraphic, lithological, and

Table 1
List of Exploration Wells Used in This Study That Are Ordered According to Ascending Total Depth

Wells	Year	Operator	Coordinates (°)		Total depth (m)	Available well logs
			Longitude	Latitude		
Al Khatt-1x	1988	IPC	55.6878	25.3341	1,524	GR, sonic
Salama-1	2003	Atlantis	56.2376	26.4370	1,582	GR, sonic
Tibat-1ST	2002	Novus	55.9709	25.5713	3,080	GR, sonic
Jazirat-Hulaylah-1x	1984	Union	56.0965	26.5864	3,127	GR, sonic
Bukha-2	1982	IPC	55.9539	26.0499	3,818	GR, sonic
Umbarek-1	1983	SEDCO	54.6715	25.6285	4,168	Sonic
Peter-1	1977	DPC	55.9774	25.4783	4,200	Sonic
Sharjah-2	1999	Crescent	55.9644	26.3970	4,430	RHOB
Hagil-1x	2006	Indago	54.9584	25.5783	4,476	Gr, NPHI, RHOB
HD-1	1973	Mobil	56.0530	26.2460	4,598	GR, sonic
HA-1	1975/1976	Mobil	56.0381	25.9154	4,600	GR, sonic
Henjam-1	1975	Elf	56.1544	26.3840	4,700	GR, sonic
Sajaa-1	1980	Amoco	56.0641	26.1279	5,028	RHOB
Ghubbali-1	1982	Elf	56.0680	25.9376	5,124	GR, sonic
Rahmah-1x	1984	Gulf	55.1996	25.6283	5,300	GR, sonic, NPHI, RHOB
Jiri-1x	1980	Gulf	56.4000	26.9500	5,318	GR, sonic, RHOB, CAL, ILS, NPHI, ILD
Aman-1	1998	RAK O&G	56.0257	25.9796	5,396	GR, sonic, RHOB

Note. Also, their locations in latitude and longitude degrees are shown and can be seen on the basemap in Figure 1.

Table 2
Compiled Formation Tops, Their Ages, and Predicted Paleobathymetry (Water Depth) From the 17 Exploration Wells

				Water depth (m)		Depth to formation tops (m)					
Age (Ma)	Era	Period	Formation tops	Min	Max	Jazirat-Hulaylah-1x	Al Khatt-1x	Salama-2	Tibat-1ST	Bukha-2	Umbarek-1
2.7	Cenozoic	Quat.	Mishan and Guri or Recent	0	100	6.4		75	48	75	168
4		Neogene	Upper Fars	0	10				98		283
15			Lower Fars	0	10		52		390		216
17.5			Gacharsah	0	10						
21			Asmari	0	100				587		
27		Paleogene	Pabdeh	200	500	1,506		650	769	500	2,431
42			Dammam	200	500						
47			Rus	200	500						
52			Umm Er Radhuma	200	500						
64	Mesozoic	Cretaceous	Simsima	100	200		658				
72.5			Fiqa	200	500	1,818/2,556	884	750		1,700	3,078
75			Ilam	200	500						3,621
79			Laffan	200	500				937		3,687
91			Mishrif	0	100				1,987		3,691
95			Shiliaf	0	100						3,761
98			Mauddud	0	100			1,050	2,544	3,025	3,819
100			Nahr Umr	100	200	2,023/2,711		1,100	2,620	3,050	3,863
104			SabSab	100	200				2,702		
108			Bab	100	200				2,736		
110			Shuaiba	100	200	2,144/2,835	1,225		2,771	3,175	3,950
115			Gaovan	100	200					3,325	
117.5			Kharaib	0	100		999	1,375	2,783	3,550	
120			Lekhwair	100	200		1,084		2,886		
125			Habshan	0	100				3,105		
130			Salil	0	100						
133			Rayda	0	100						
136		Jurassic	Hith	0	10					3,700	
146			Diyab	0	100						
157			Araej	0	10						
165			Izhara	0	100						
168			Hamlah	100	200						
180			Marrat	0	100						
—			Thrust	-	0						
189			U. Minjur	0	10						
196		Triassic	Ghalilah	0	100						
208			Milaha	0	100						
237			Ghail	0	100						
250			Sudair/Hagil	100	200						
255	Paleozoic	Permian	Bih/Khuff	0	10						
260			Paleozoic?	200	500						

Note. Note that few formations from Hagil-1x, Ghubbali-1, and Jazirat-Hulaylah-1x wells have two depth values resulted from repetition caused by thrusting associated with the Hagab thrust.

paleoenvironmental analyses carried out on samples from the Aman-1, Rahmah-1x, Sajaa-1, Jazirat-Hulaylah-1, and Al Khatt-1x wells were used to identify the paleobathymetry of each formation. If the well reports did not have this information, as in the Tibat-1ST, Hagil-1x, and Jiri-1x wells, we referred to core descriptions of the lithologies that are then used to infer whether the water depth was shallow, moderate, or deep using the classification of Heller (1983). There are a number of wells where both sources are absent (Salama-1, Bukha-2, Umbarek-1, Peter-1, Sharjah-2, HD-1, HA-1, Henjam-1, and Ghubbali-1). In these cases, we used the paleobathymetry data obtained from nearby wells. The data were compared with the paleobathymetric maps of Ziegler (2001), which capture the water depth evolution throughout the Arabian plate since the Late Permian. In general, the paleobathymery data of exploration wells agree with the paleobathymetric maps with the exception in the Triassic where Ziegler (2001) predicts a deep water environment in the Musandam peninsula.

Table 2 *(continued)*

	Depth to formation tops (m)										
Age (Ma)	Peter-1	Sharjah-2	Hagil-1x	HD-1	HA-1	Henjam-1	Sajaa-2	Ghubbali-1	Rahmah-1x	Jiri-1x	Aman-1x
2.7	168	168	5	75	75	75		75	7		48
4	283	283									98
15	500	524		875	875	875					390
17.5				1,225	1,225	1,225	91				
21				1,700	1,575		140				587
27	1,902	2,601		2,075	1,950	1,500	274	500	103	28	769
42	2,284	3,119					945				
47							1,463				
52	2,550						1,591				
64							2,006		200		
72.5	2,693	3,464		2,175	3,875	3,000	2,231	575/2,625	295		
75	3,084	3,084		3,575	4,250		2,396		4,395		
79	3,163						2,865		4,402		3,937
91	3,166	3,166			4,275	3,775		950			4,987
95	3,317	3,317									
98	3,324	3,324		3,585	4,325	3,975		1,000/4,325	4,405		5,032
100	3,392	3,392	8	3,700	4,450	4,025	3,048	1,050/4,400	4,420		5,039
104									4,535		5,131
108									4,545		5,146
110	3,478	3,478	72	3,850	4,505	4,100	3,121	1,175/4,500	4,577		5,181
115				3,950		4,200		1,425			
117.5			134	4,025		4,500	3,267	1,625	4,615		5,201
120			234						4,735		5,266
125			384				3,627		5,237		
130			565								
133								1,875		67	
136	4,131		635	4,125			4,097			476	
146			689				4,133			551	
157							4,365			616	
165			763				4,532			802	
168			1,180				4,618			1,151	
180								2,475			
—			1,880								
189			1,306.6/1,964.4				4,755			1,494	
196			1,391.1/1,966.6				4,822			1,928	
208			1,600/2,180				4,907			2,308	
237			1,669.7/2,383.5							2,652	
250			1,746.8/2,653.2							3,344	
255			1,850.4/2,851.7							3,743	
260			3,665								

5.2.4. Eustatic Sea-Level Change

When backstripping well data, we need to correct for the effects of loading and unloading of water due to sea-level change. The deepest available wells in the western Musandam peninsula penetrate the Upper Permian (Hagil-1x and Jiri-1x). However, the amplitude of sea-level change since the Late Permian is not well known (Figure 11a). In this study, we corrected for sea level using the long-term sea-level curves of Watts and Steckler (1979), Haq and Al-Qahtani (2005), and Haq and Schutter (2008; Figures 11b–11f). The correction was tested on one of the deepest wells, Hagil-1x, which penetrated thrust-induced repeat sequences.

The tectonic subsidence and uplift calculated using a combination of the long-term sea-level curves of curve of Watts and Steckler (1979) and Haq and Al-Qahtani (2005) yields a smooth tectonic subsidence curve that appears to capture the primary controlling tectonic mechanisms (Figure 11c). We therefore selected this curve to correct the effect of sea-level change for all the wells. Other sea-level curves

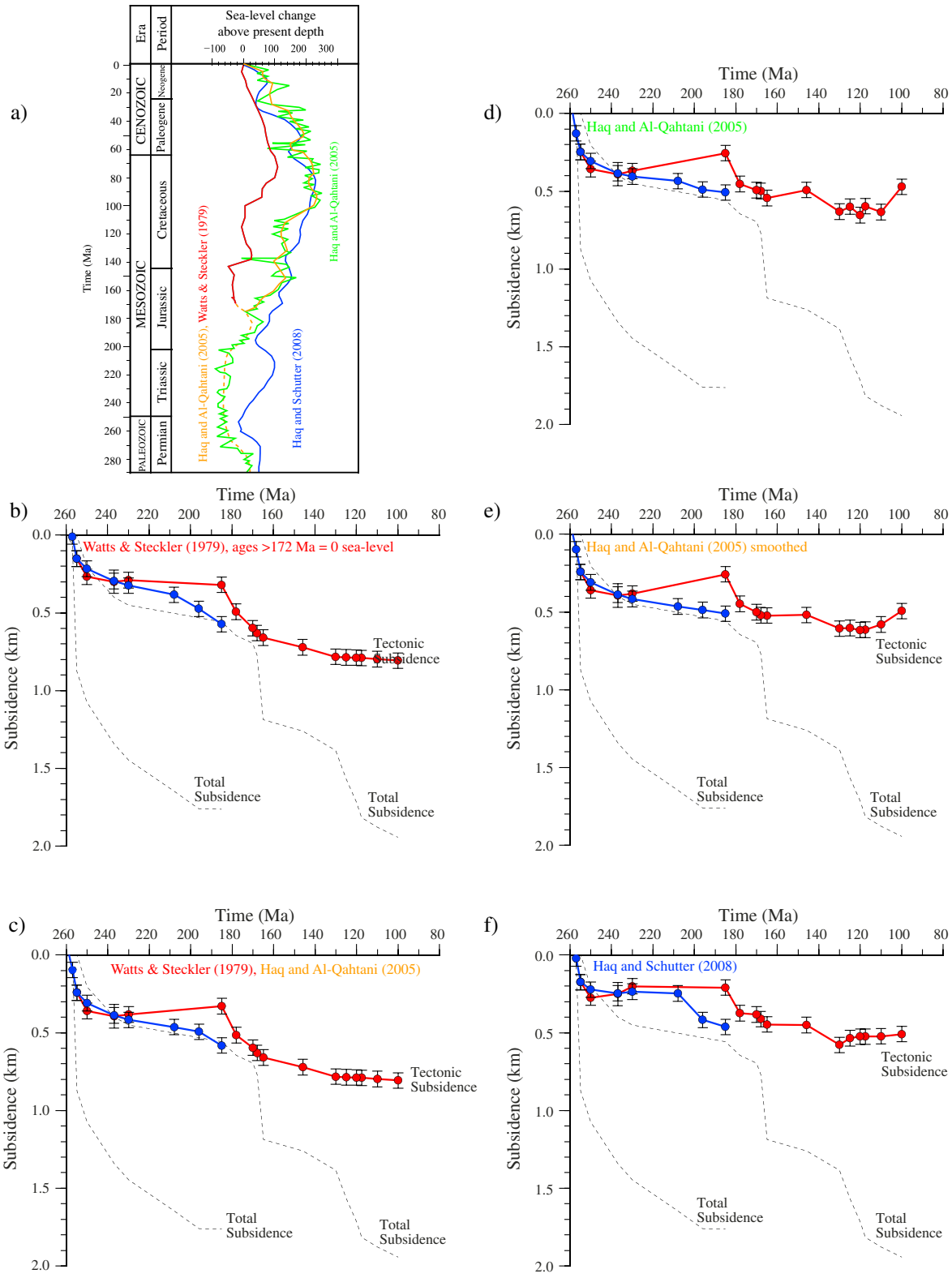

Figure 11. (a) Sea-level curves tested to construct the tectonic subsidence curves of Hagil-1x as shown in Figures 11b–11f in Hagil-1x. A composite of the Watts and Steckler (1979) and Haq and Al-Qahtani (2005) sea-level curves was selected in order to capture regional changes in the tectonic subsidence and uplift (red and smooth dashed orange curves are Watts & Steckler, 1979; Haq & Al-Qahtani, 2005, sea-level curves, respectively). Green sea-level curve of Haq and Al-Qahtani (2005) was smoothed using a moving average method. Note the tectonic subsidence curves show thrust-induced repeat sequences. Blue and red curves show the tectonic subsidence for sediments below and above the Hagab thrust.

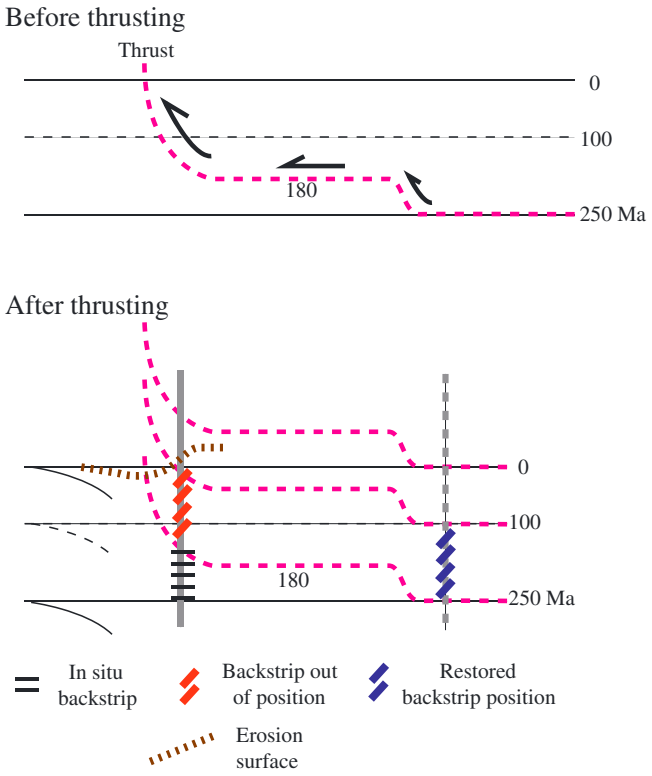

Figure 12. Schematic diagram showing how a hypothetical well (solid gray line) that penetrates a thrust that is composed of two backstrip curves: one below the thrust that is "in situ" and reflects the tectonic subsidence and uplift at the well and another above the thrust that has been displaced laterally and reflects the tectonic subsidence and uplift at a distal position (dashed gray line).

capture short-term changes and result in unrealistic changes of tectonic subsidence and uplift (Figures 11d and 9f). The smooth global curve of Watts and Steckler (1979) has been shown by Miller et al. (2005) to be representative of the long-term sea-level change during the Mesozoic and Cenozoic. The Haq and Al-Qahtani (2005) curve extends the long-term sea-level record into the Paleozoic. The curve was deduced from data acquired on the Arabian plate including sections from Saudi Arabia, Kuwait, the Arabian Gulf area, Oman, and Yemen using onlaps and erosional surfaces. The curve was smoothed to capture the effects of regional tectonics (dashed line, Figure 11a).

5.3. Thrusting and Repeat Sequences

We note that the Hagil-1x, Ghubbali-1, and Jazirat-Hulaylah-1x wells have two depth values for some formation tops indicating repetition of the stratigraphy due to stacking along the Hagab thrust. For example, the Hagil-1x well (Figures 7 and 11b–11f) encountered the Hagab thrust that repeats the Rus al Jibal, Elphinstone, Musandam, and Thamama Groups. The backstrip derived from the sedimentary sections above and below the thrust will not therefore apply to the same location along a cross section. This is illustrated schematically in Figure 12, which shows for a theoretical well that the backstrip from above the thrust has been displaced laterally while the backstrip from below the thrust is in situ.

Figures 11b–11f show the separate backstrips for the sediments above and below the Hagab thrust. The solid red line shows the backstrip for the sedimentary section above the thrust, while the solid blue line shows the backstrip for the section below the thrust. Despite the lateral offset in the two backstrips (which we estimate based on the restored sections in Figure 8 to be ~5 km), Figures 11b–11f show close agreement in the early tectonic subsidence at the Hagil-1x well (note that the blue backstrip curve overlies the red backstrip curve for ages of 260–250 Ma). After ~230 Ma, the two curves start to deviate, and the section above the thrust reveals an abrupt increase in tectonic subsidence at ~180 Ma.

5.4. Subsidence and Uplift History

5.4.1. Tectonic Subsidence

Figure 13a shows the total and tectonic subsidence curves for the Jiri-1x well. The well penetrated an almost complete Upper Permian to Lower Cretaceous sequences. The bottom dashed line shows the total one-dimensional tectonic subsidence, which is composed of a subsidence due to sediment and water loading, and the unknown tectonic driven subsidence. The error bars on the tectonic subsidence curve indicate uncertainties in the paleobathymetry and sea-level estimates.

All 17 wells were backstripped, and distinct events in the tectonic subsidence and uplift were identified using a similar approach as shown in the Jiri-1x well (Figures 13a–13n). Wells located close to each other were correlated to capture the main tectonic events. However, onsets of tectonic events vary slightly from well to well. Hagil-1x, Sajaa-1, and Henjam-1x wells were chosen as representatives of the 17 wells. This allowed us to produce, in effect, a continuous tectonic subsidence and uplift curve from the Late Permian up to the present day (Figures 14a–14c). As a result, we have been able to identify two rifting and two compressional events in the tectonic subsidence of the western Musandam peninsula region.

5.4.2. Late Permian and Early Jurassic Rifting Events

Only three wells were drilled deep enough to penetrate the Permian to the Late Cretaceous rift sequences. The Hagil-1x and Jiri-1x wells fully capture the two rifting episodes, while the Sajaa-1 well includes only the last episode of rifting (Figures 13a, 14a, and 14b). The other wells only record part of the second rifting event (Figures 13b–13n). The Hagil-1x and Jiri-1x wells indicate two rifting events that are separated in time by ~70 Myr. The tectonic subsidence associated with each event is concave up with an initial rapid

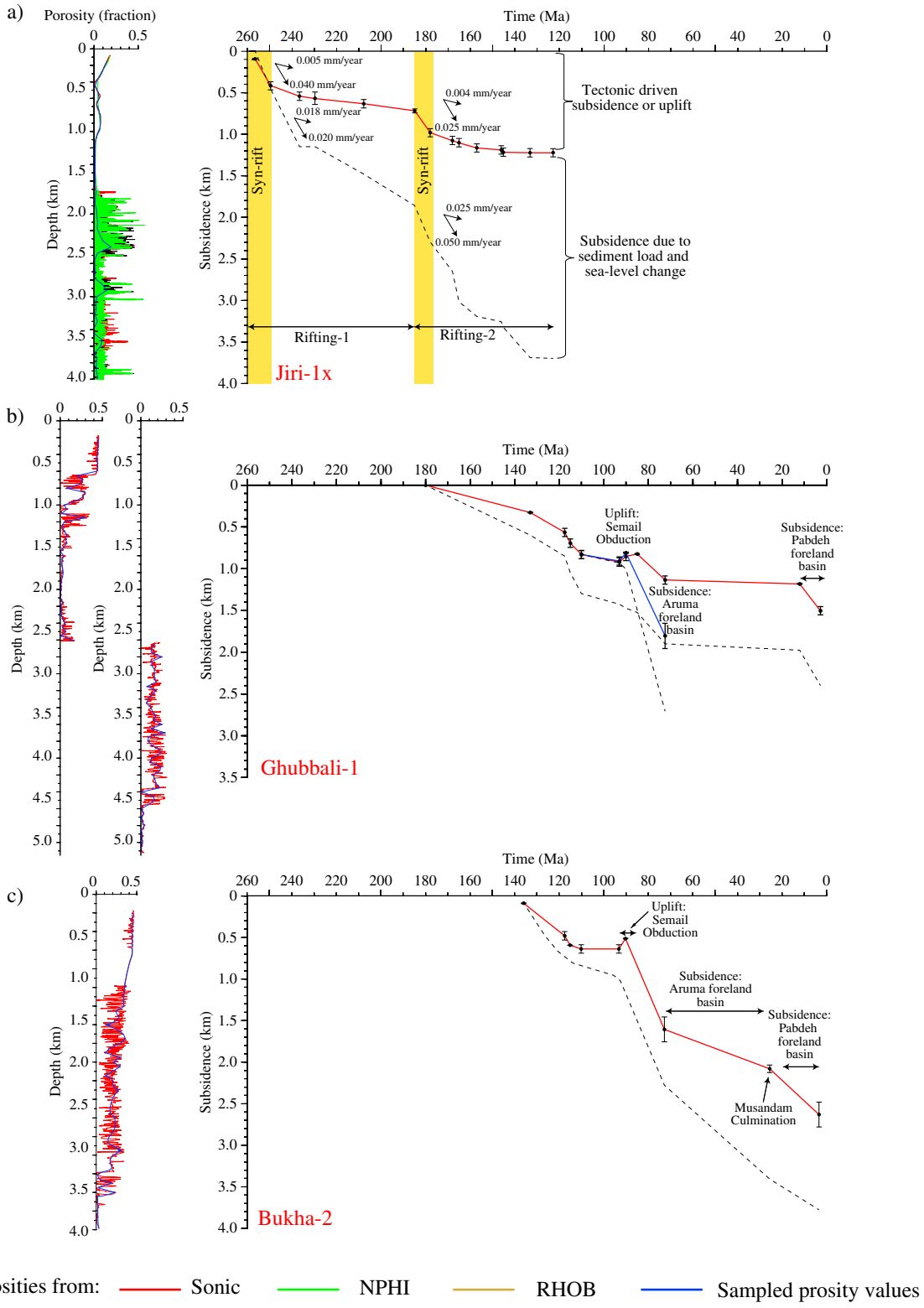

Figure 13. (a–n). Backstripped wells in the western Musandam peninsula (refer to Figure 1 for locations). The backstripped curves are correlated according to their tectonically driven subsidence shapes. The backstripped curves are plotted along with depth–porosity profiles used to constrain the decompacted thickness of sedimentary layers. Note that arrows on Jiri-1x well indicate the syn-rift and postrift subsidence rates.

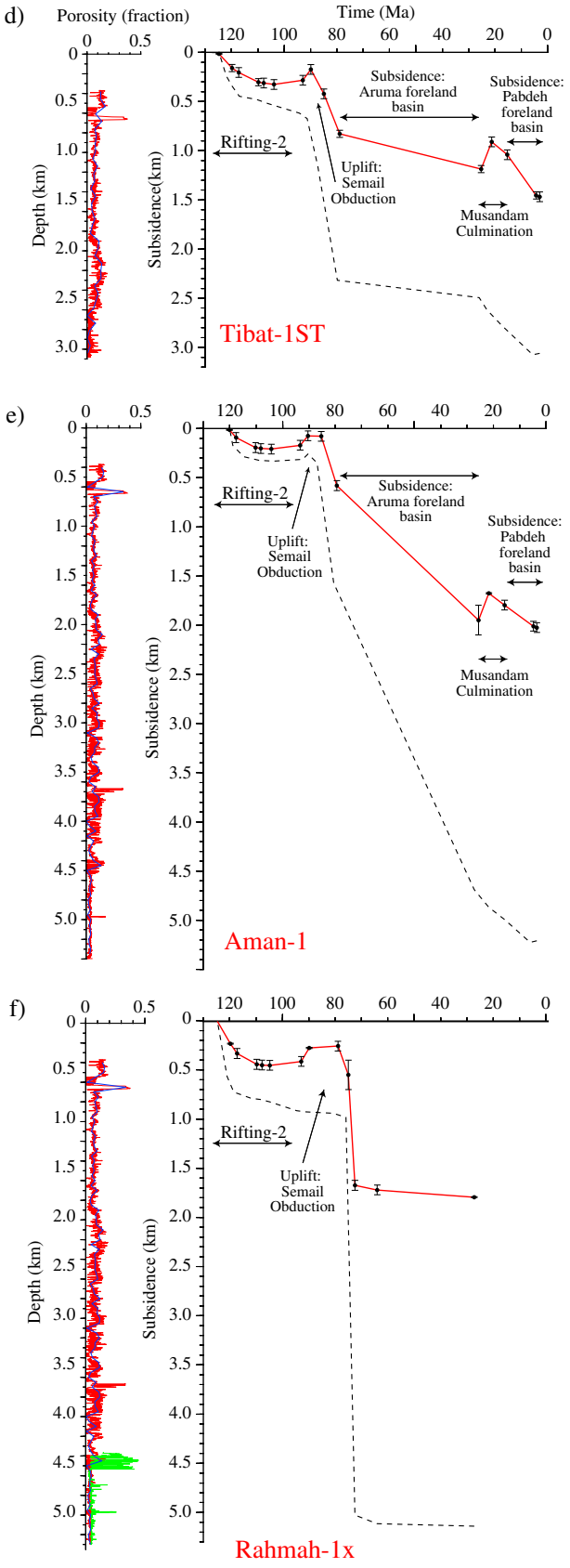

Figure 13. (continued)

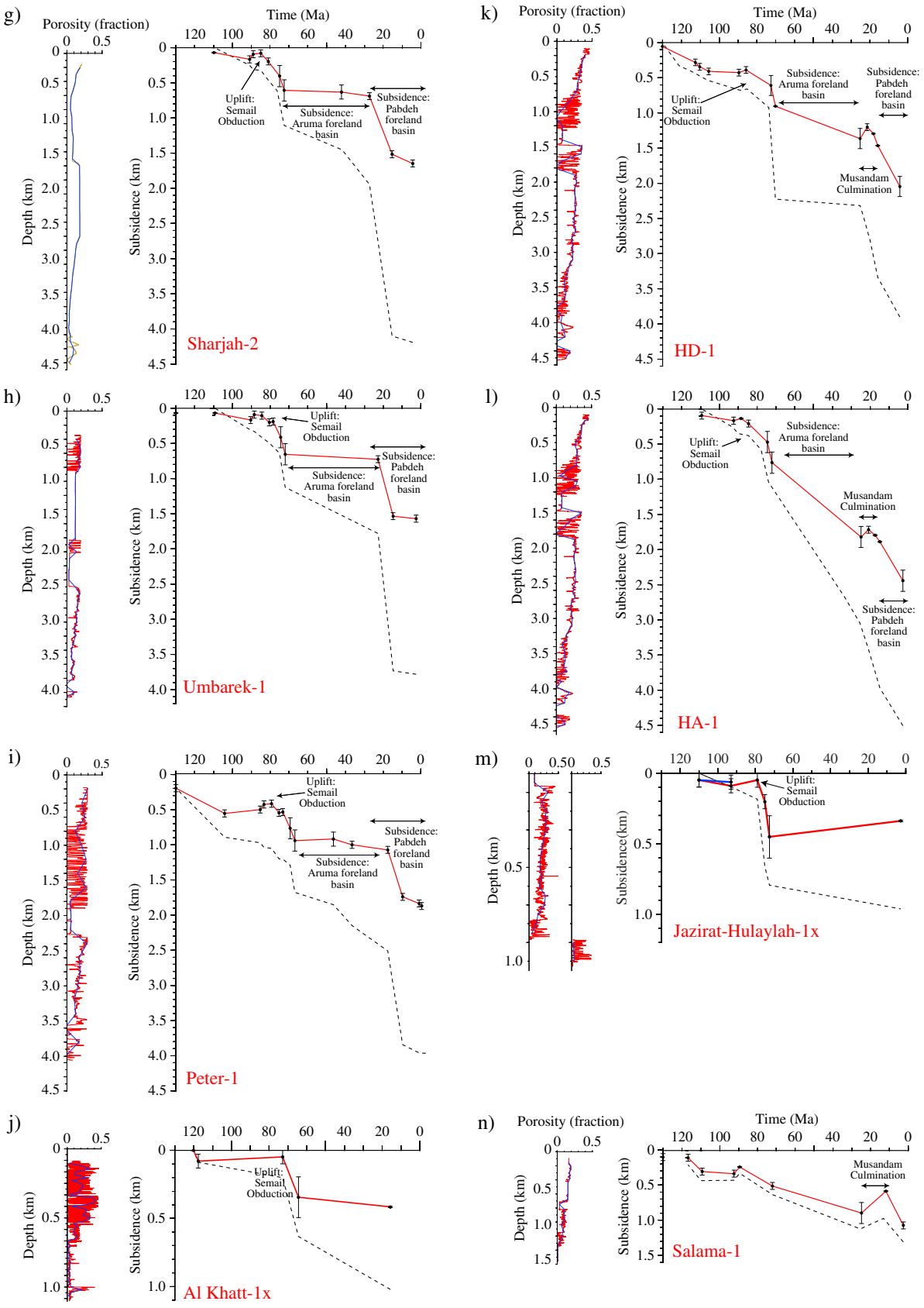

Figure 13. (continued)

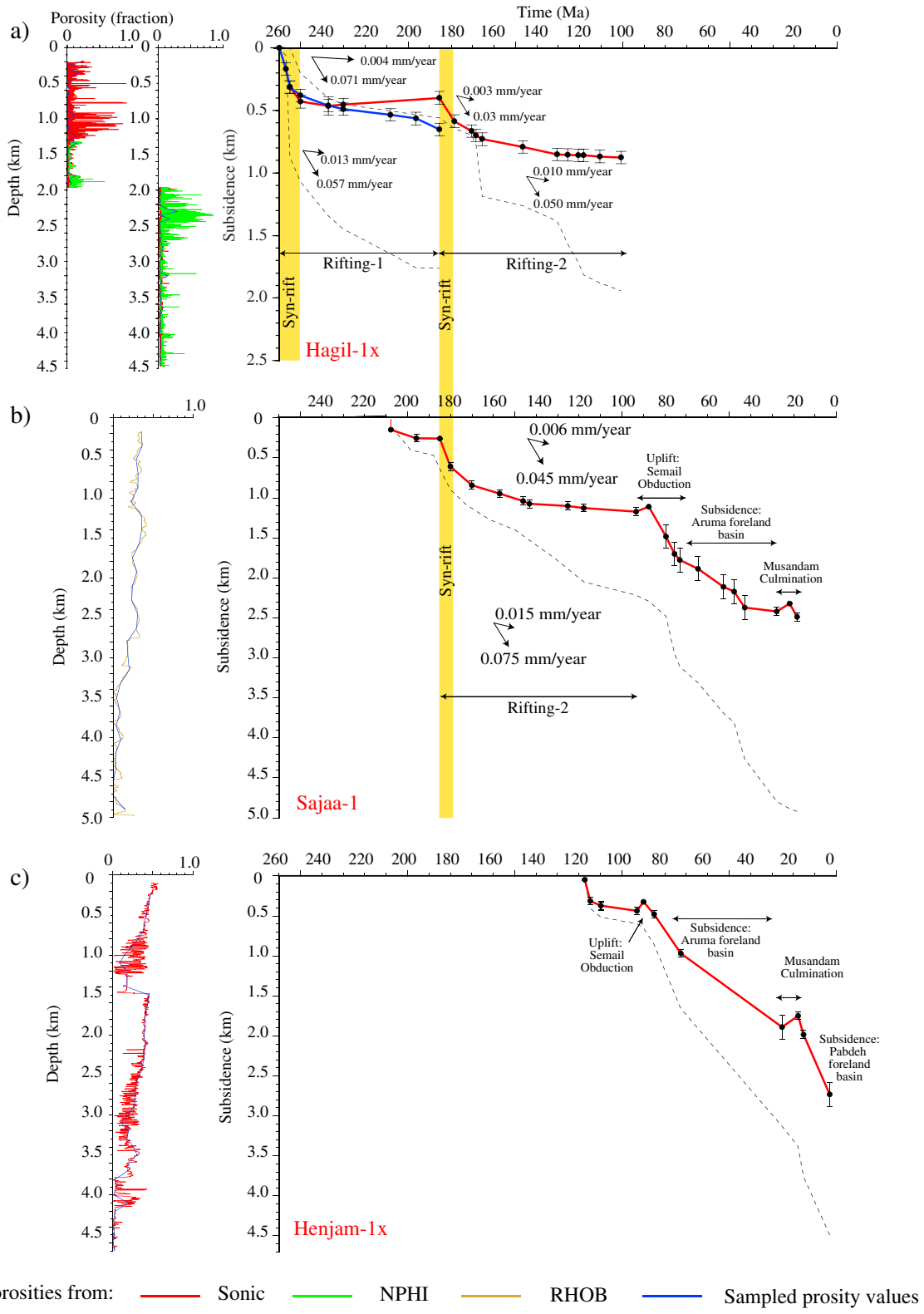

Figure 14. A correlation of three representative wells (Hagil-1x, Sajaa-1, and Henjam-1x), which forms continues subsidence/uplift history since the Late Permian up to the present day. Note that Hagil-1x well penetrated repeated stratigraphy where both stratigraphic stacks capture similar subsidence trends. The compiled trend of subsidence curves heralds the main tectonic events evolved within the Musandam peninsula area. Arrows on the Hagil-1x and Sajaa-1 wells show amount of syn-rift and postrift subsidence, tectonic driven, and sediment/water loading. Porosity–depth curves on the left side are used to construct the decompacted sediment thickness of buried stratigraphic layers (bottom most dashed line).

Table 3
Parameters Used in the Thermal and Mechanical Models

Parameter	Definition	Value/unit
a	Lithospheric thickness	125 km
T_c	Crustal thickness	Max 31.2 km (vary)
ρ_{lo}	Density of lithosphere at 0°C	Max 3,330 kg m^{-3} (vary)
ρ_{co}	Density of crust 0°C	2,800 kg m^{-3}
ρ_w	Density of water	1,030 kg m^{-3}
T_m	Temperature at base of lithosphere	Max 1,330°C (vary)
α	Coefficient of volume expansion	3.28×10^{-5}°C^{-1}
β	Stretching factor	Vary as required

subsidence followed by an exponential postrift subsidence. The first rifting event starts from ~260 Ma. The Hagil-1x well shows that the syn-rift stage has a higher subsidence rate of 0.071 mm/yr in comparison with the postrift stage (300 m and 0.004 mm/yr; Figure 14a). The total subsidence varies among wells between 2,100 and 2,200 m, which is composed of 700–800 m of tectonic-driven subsidence and 900–1,300 m of sediment and water loading subsidence (Figures 13a and 14a).

The second rift event that initiated at ~185 Ma lasted for ~10 Myr and resulted in ~250–450 m of tectonic subsidence. At this syn-rift stage, the lithosphere subsides with the rate of 0.025–0.045 mm/yr (Figures 13a, 14a, and 14b). At the postrift stage, the tectonic subsidence rate decreases to 0.003–0.006 mm/yr (Figures 13a, 14a, and 14b). The subsidence governed by the sediment and water loading has a similar trend. It starts with high rates of subsidence between 0.050 and 0.075 mm/yr during the syn-rift stage and declines to 0.010–0.025 mm/yr rate at the postrift stage (Figures 13a, 14a and 14b).

5.4.3. Late Cretaceous Uplift and Subsidence Event

Almost all of the wells document an uplift event that started at ~94 Ma and ended at ~80 Ma. Onset of this convex up shaped uplift in distal offshore wells from the load of Semail Ophiolite (Peter-1, Umbarek-1, and Sharjah-2; Figures 13g–13i) appears to be recorded ~2 Myr later (~92 Ma) than the wells located in the proximal area (e.g., Bukha-2, Tibat-1ST, Aman-1, and Rahmah-1x; Figures 13–13f). Immediately after the uplift (between ~80 and 70 Ma), the crust experiences a rapid subsidence with up to 1.8 km of tectonic subsidence (Figure 14c).

5.4.4. Oligocene–Miocene Uplift and Subsidence Event

A convex up shape in the tectonic subsidence is evident with a time span between ~25 and ~20 Ma. This phase of uplift is particularly evident at the Aman-1, Tibat-1ST, HD-1, HA-1, Salama-1, Sajaa-1, and Henjam-1 wells drilled along the Hagab thrust (Figures 13d, 13e, 13l, 13m, 13n, 12b, and 12c). This event was followed by tectonic subsidence of up to 1 km (Figure 13e).

5.5. Multirift Uniform Stretching Models

We used a multirift, finite rift duration, uniform stretching model (Cochran, 1981) along with the parameters given in Table 3 to determine the amount of crustal and lithospheric extension at the well locations. The model quantitatively separates the initial fault controlled syn-rift subsidence from the subsequent postrift thermal subsidence driven by the cooling of the lithosphere.

We compared the tectonic subsidence and uplift curves at the Hagil-1x, Jiri-1x, and Sajaa-1 wells to predictions of the thermal model with different values of the amount of crust and mantle stretching, β. Two rifting events were assumed. An initial rifting that started at 260 Ma and a second rifting phase that started at 185 Ma. Furthermore, the tectonic subsidence and uplift were shifted vertically until a satisfactory fit was achieved between model calculations and the observed tectonic subsidence and uplift. This takes into account the fact that Sajaa-1 and Hagil-1x (second thrust) wells did not penetrate the syn-rift sediments of the first rifting episode. Finally, a root mean square (RMS) analysis was used to determine the best-fit β factor between observed and calculated tectonic subsidence and uplift curves (Figures 15a–15c).

5.5.1. First Rifting Event

Only two wells, Hagil-1x and Sajaa-1, were drilled deep enough to penetrate a syn-rift sequence corresponding to this rifting event. The syn-rift stage starts at ~255 Ma with ~5 to ~7 Myr of rift duration (Figures 15a and 15b). The comparison between observed and predicted tectonic subsidence curves shows that the crust stretched with a β factor of 1.09 at the Hagil-1x and Jiri-1x wells (Figures 15a and 15b).

5.5.2. Second Rifting Event

All three deep wells (Hagil-1x, Jiri-1x, and Sajaa-1) show tectonically driven subsidence curves of the second rifting episode, which was initiated in mid-Jurassic with rift duration of ~10 Myr (Figures 15a–15c). Since this rifting episode has followed the precursor first rifting event, the assumed crustal thickness has already been stretched and thinned by the first rifting event. Accordingly, the second rifting at Hagil-1x, Jiri-1x, and Sajaa-1 wells has a prerift crustal thickness of 28.6 km. The crustal thickness for the rifting models in the Sajaa-1 well was extracted from the nearest well, Jiri-1x. The RMS analysis (Figures 15a–15c) at the Hagil-1x, Jiri-1x, and

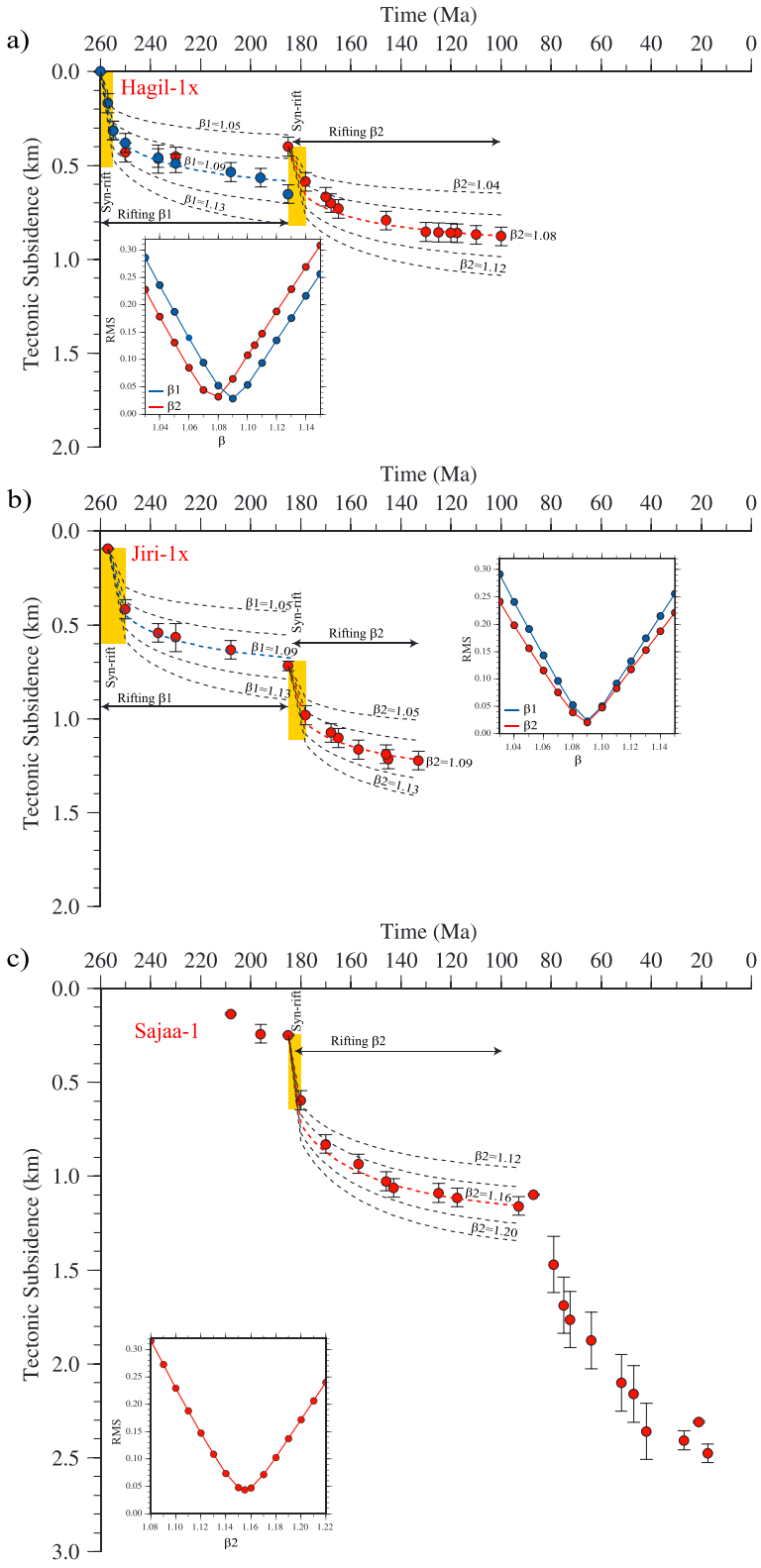

Figure 15. A set of uniform stretching models compared with observed tectonic subsidence curves for (a) Hagil-1x, (b) Jiri-1x, and (c) Sajaa-1 (For locations see Figure 1). Insert in Figure 15a shows RMS calculations for Hagil-1x with best-fit β values of 1.09 and 1.08 for rifting episodes 1 and 2, respectively; insert in Figure 15b shows RMS for Jiri-1x with best-fit β value of 1.09 for both rifting episodes; insert in Figure 15c shows the β value of 1.155, which explains the observed tectonic subsidence curve of Sajaa-1.

Sajaa-1 wells suggests best-fit β values of 1.08, 1.09, and 1.155, respectively, which thinned the crust to 26.5, 26.3, and 24.8 km at each well, respectively.

6. Discussion

6.1. Stratigraphy and Structures of Western Musandam Peninsula

Seismic reflection and well data show that the subsurface stratigraphic architecture of the western side of the Musandam peninsula can be divided into five main "megasequences": (1) Permian–Cretaceous shelf carbonates, (2) Late Cretaceous Aruma foreland basin sequence, (3) early–mid-Cenozoic Pabdeh foreland basin sequence, (4) late Cenozoic sequence (Fars Group), and (5) late Pliocene sequence (Mishan and Guri Formations).

The Permian–Cretaceous megasequence consists of Permian Bih and Hagil Formations, Triassic–Jurassic shelf carbonates (Ghail, Milaha, Ghalilah Formations, and Musandam Group), and Lower Cretaceous to Cenomanian shelf carbonates (Thamama and Wasia Groups). However, it was not possible to image clearly the Permian sequence due to limited well control, complexity of structures, and poor quality of the seismic data. The Jiri-1x well penetrated 3,267 m of the Triassic–Jurassic sediment (Table 2). To the south, in front of the northern Oman mountains, the thickness of the Triassic–Jurassic sequence is estimated to be at least 4 km (Ali et al., 2013). The top of the Cretaceous shelf carbonates (top of the Wasia Group) is an erosional surface known as the Wasia–Aruma "break," which probably resulted from a flexural bulge associated with the initial onset of the emplacement of the Semail Ophiolite in the Late Turonian (Ali, Sirat, & Small, 2008; Patton & O'Connor, 1988). Overall, the Cretaceous shelf carbonates thin from ~1.6 km (0.8 s TWT; Lines 3, 4, and 5 on Figures 5b and 6b) to ~1.2 km (0.6 s TWT; Line 1 on Figure 4b) toward the northeast, where the Wasia–Aruma erosion is more pronounced. To the southeast, close to the Jiri-1x well (Line 6 on Figure 6b), the Wasia and Aruma Groups are missing, and the Thamama Group is only 409 m thick due mainly to a subsequent late Oligocene–early Miocene uplift event (Searle et al., 2014).

In the southeast of the study area, the thickness of the Late Cretaceous Aruma foreland basin sequence reaches up to ~2 km (~1.0 TWT; Figure 6b), while it reaches ~2.5 km (~1.25 TWT) on seismic profile D4 as interpreted by Tarapoanca et al. (2010; Figure 1 for location). On the contrary, the Aruma Group thins to ~1 km (~0.5 TWT) toward the north (Figures 4b and 5b). Wireline logs indicate that the sequence consists of tight deep-water sediments with porosities ranging between ~5% and 10%. For example, Aman-1 well penetrated a thick sequence of Aruma Group consisting of interbedded claystone, shale, and limestone. Toward the base of the sequence, shale is the predominant lithology, interbedded with thin limestone. In addition, the Rahmah-1x well encountered over 4,100 m of imbricate fine clastics of the Aruma Group, which unconformably overlie the middle Cretaceous Nahr Umr Formation. Furthermore, none of the wells located at the western edge of the Musandam peninsula penetrate the Simsima Formation, which is composed of transgressive shallow marine carbonates of Late Maastrichtian age (Searle & Ali, 2009). However, the Simsima Formation is recorded further to the south (Sajaa-1 well) where the late Oligocene–early Miocene deformation event has less impact.

The internal characteristics of the early–mid-Cenozoic Pabdeh foreland basin sequence, especially that close to the Hagab thrust, have a chaotic seismic expression indicating an accumulation of high energy mass wasting deposits such as rock breccia as was encountered in the Rahmah-1x well (Johnson, 1985). The chaotic patterns represent discontinuous and discordant reflectors suggesting a disordered arrangement of reflection surfaces. The maximum thickness adjacent to the Hagab thrust reaches up to ~4 km (2.0 s TWT) and thins to ~800 m (~0.4 s TWT; D4 from Tarapoanca et al., 2010) in a wedge shaped to the west of the Musandam peninsula. The Aman-1 well penetrated 3,170 m of Pabdeh Group consisting of claystone with chert, conglomerate, and limestone. Moreover, the Brooze-1 well penetrated a thick Cenozoic flysch sequence overlying a thrust sequence of Upper Cretaceous pelagic limestone. The thickness of the Pabdeh sequence exhibits a small reduction (~3 km) to the south in the vicinity of Jabal Sumeini at the UAE–Oman border (Ali et al., 2013).

The seismic stratigraphy described above suggests that the internal structure of the Pabdeh foreland basin is characterized by a wedge-shaped geometry that tapers away from the mountain front. We therefore suggest that the basin was formed due to flexure of orogenic loads in the Musandam mountains. These loads developed during an early stage of continent–continent collision along the Zagros suture zone as the Arabian plate

Table 4
Stratigraphic Tops and Average Dip at the Jiri-1x Well

Formation	Top (m)	Average dip (°)	Faults (m)
L. Tertiary	0	0	
Pabdeh	28	5	
Rayda	67	33	
		32	
Hith	476	40	
Diyab	551	33	
		35	
Araej	616	32	Possible 575
Izhara	802	34	
Marrat	1,151	36	
U. Minjur	1,494	46	Probable 1,713
Ghalilah	1,928	40	Probable 1,957
Milaha	2,308	39	Probable 2,338
			Possible 2,475
Ghail	2,652	35	Possible 2,719
			Possible 3,283
Hagil	3,344	37	Possible 3,428
			Possible 3,634
Bih	3,743	53	Possible 3,954
			Possible 4,319
			Possible 4,533
			Possible 4,754

Note. Faults are detected from the dipmeter and sonic data (Johnson & Frost, 1981).

began to collide with the Eurasian plate along the Iran–western Makran continental margin (Searle & Ali, 2009). Furthermore, the localized anticlinal-shaped uplifts in Lines 3 and 5 suggest that deposition of the Pabdeh Formation was contemporaneous with the thrust and folding event (Figures 5b and 6b).

The internal seismic reflectors of the late Cenozoic sequence (Fars Group) are continuous and appear as flat lying. These characteristics are consistent throughout the seismic profiles, and we interpret them as cyclic salts of the Lower Fars Group, which were deposited during opening of the Strait of Hormuz (Ricateau & Riche, 1980). Wells drilled offshore Sharjah (Peter-1, Umbarek-1, and Sharjah-2; Figure 3c) documented thick salt (~1 km) of the Fars Group that was deposited in an intertidal environment with much less connection to the open sea. Furthermore, the Aman-1 well penetrated cyclic salt consisting of a sequence of anhydrite interbedded with claystone. The flat-lying geometry of the sediments suggests that the accommodation space was probably created due to flexure driven by the continuation of orogenic loads associated with the early–mid-Cenozoic Musandam culmination (Figure 8).

The thickness of the late Pliocene sequence ranges from ~500 m (0.25 s TWT; Figure 4b) at the shoreline of the western Musandam peninsula to ~1,000 m (0.5 s TWT; Figure 4b) in the northwest Arabian Gulf. This observation is explained by the ongoing subsidence due to flexure that was initiated in the early–mid-Cenozoic and continued into the latest stage of continent–continent collision between the Arabian and Eurasian plates in central Iran. This sequence was interpreted as sediments of Guri conglomerates at the base and Mishan marls at the top. The sequence overlies the late Pliocene unconformity, which we interpret as tilting due to the latest stage of continent–continent collision between the Arabian Eurasian plates along the Zagros suture zone (Koop & Stonely, 1982; Searle et al., 2014).

6.2. Structural Style of the Hagab Thrust

All seismic profiles of the Hagab thrust capture the late Oligocene–early Miocene compressional deformation of folding and west-verging thrusting that resulted in the Musandam culmination. The seismic data show that the majority of the thrusts terminate below the mid-Miocene unconformity, which separates from the overlying evaporitic sediments of the Fars Group and marks the end of the compressional Oligocene–Miocene Musandam culmination event (Jahani et al., 2009). The observations from the seismic data are in agreement with the well and surface geology where the Oligocene–early Miocene compressional event initiated thrusting of up to 4 km mid-Permian to Cenomanian shelf carbonates along the west-verging Hagab thrust. The Jazirat-Hulaylah-1x, Ghubbali-1, and Hagil-1x wells are drilled along the Hagab thrust and penetrated repeated sequences (Table 2). These thrusts offset the Permian to Upper Cretaceous shelf carbonates by up to ~1 km (0.5 s TWT; Figures 4b, 5b, and 6b).

Moreover, the Jiri-1x well was drilled in a complex area of a large anticlinal feature below a series of imbricate thrust sheets (Figure 6b). Dipmeter data and regional geological interpretation suggest that the well was drilled into the westward dipping limb of a south-plunging frontal fold located in the distal portion of the Hagab thrust sheet (Johnson & Frost, 1981). The dip of the fold increases downward in the well, as does the intensity of faulting and fracturing (Table 4).

In addition, the Hagil-1x well was drilled along the Hagab thrust. The well penetrated two repeated thrusts within a significant mylonite and a complex lower Paleozoic mélange (Indago-Petroleum, 2006). The thrusting placed Upper Permian sequences over Triassic (Figure 7). The upper thrust is composed of a succession from Lower Cretaceous to Permian, and the lower thrust sheet consists of a succession from the Upper Triassic to the Lower Permian. A significant (823 m) Triassic section is missing from the upper thrust sheet. Indago-Petroleum (2006) suggested that the missing section is due to the erosion of the upthrown Triassic

extensional fault block. However, there is no evidence of large extensional faults both from seismic and outcrop data.

Furthermore, the balanced and restored cross sections (Figures 8 and 9) show that the Oligocene thrusting of the Musandam peninsula was a thick-skinned event with thrusts that involved the pre-Permian basement. Oligocene thrust tip lines are truncated by a prominent regional unconformity along the base of the Miocene Fars and Mishan Formations. The total amount of crustal shortening is minor (between 8 and 15 km minimum), but crustal thickening is more prominent. The Musandam culmination is cut by a very large-scale ESE-dipping normal fault, the Dibba fault, which drops the Dibba zone and Semail ophiolite down to the east. The entire Musandam peninsula was uplifted since the base Miocene and the structures are interpreted as the first effects of the Arabia–Eurasian collision (Searle, 1988b; Searle et al., 2014).

6.3. Tectonic and Uplift History of Western Musandam Peninsula

The backstripped subsidence and uplift history suggest that the western Musandam peninsula experienced two rifting events punctuated by periods of slower subsidence or uplift. The first rift phase initiated ~260 Ma with a rift duration of ~5–7 Myr and a stretching value, β, of 1.09. This stage was followed by an exponential postrift subsidence stage related to conductive cooling following initial heating and a possible uplift and erosion in the Late Triassic–Early Jurassic (Figures 15a and 15b). This was followed by a second rift event that started from ~185 Ma with rift duration of ~10 Myr and β values of 1.08, 1.09, and 1.155 for Hagil-1x, Jiri-1x, and Sajaa-1, respectively (Figures 15a–15c). These subsidence phases are broadly in agreement with some previously published estimates. A number of studies (e.g., Bechennec et al., 1990; Glennie et al., 1974; Robertson, 1986; Robertson & Searle, 1990; Searle et al., 1990) documented rifting episodes in the Late Permian and Late Triassic–Early Jurassic as a result of the continental breakup of Gondwana and opening of the Neo-Tethys Ocean. Furthermore, rapid subsidence interrupted by periods of slower subsidence or uplift was observed on the southern and northern Neo-Tethyan margin (e.g., Ellouz et al., 2003; Hanne et al., 2003; Le Nindre et al., 2003; Patriat et al., 2003; Stampfli et al., 1991). Moreover, Maurer et al. (2008) recognized a Late Triassic period of shelf exposure and erosion in the Wadi Bih area of Musandam mountains. The hiatus spans from the Carnian to the Norian (between the Ghail and Milaha Formations) and can be correlated with the possible uplift event in the Late Triassic observed in the tectonic subsidence curves. In addition, a Late Triassic (Norian) angular unconformity in the Rub' Al-Khali, southwest of the Musandam peninsula, is documented in Stewart (2016) and Stewart et al. (2016). The unconformity is characterized by an absence of the Minjur Formation.

The β value of the first rift indicates that the crust thinned to 28.6 km, assuming an initial crustal thickness of 31.2 km. We justify this thickness as it is the zero elevation thickness of the crust derived by Cochran (1981) when isostatically balancing a 125 km thick column of continental lithosphere with a mid-ocean ridge column. We do not know, of course, the thickness of the Arabian plate crust at the time of the first rift event. However, a histogram of the crustal thickness data compiled in CRUST2.0 (Bassin et al., 2000) and the GEBCO topography reveals that crust within ±200 m of mean sea level has two peaks: one at 30–32 km and the other at 38–40 km. The most prominent peak is at 30–32 km, and since Cochran's value is within this range, we have selected it here for the assumed initial crustal thickness. The amount of crustal and mantle extension of the second rifting episode implies a present-day depth-to-Moho of about 37.5 km, 37.3 km, and 35.8 km beneath the Hagil-1x, Jiri-1x, and Sajaa-1 wells, respectively (26.5 km, 26.3 km, and 24.8 km + 11 km of assumed sediment fill). Unfortunately, there is no published refraction derived crustal thickness in the study area to compare it with our estimates.

The uniform extension models are not able to explain all the features of the backstrip curves (Figure 15c). In particular, the models cannot account for the uplift and subsequent subsidence that began ~94 Ma and ~80 Ma, respectively. The uplift corresponds in time to the emplacement of the Semail Ophiolite and its associated thrusts. We therefore attribute the uplift and excess subsidence to the orogenic loading associated with flexure of the underlying rifted margin, which formed the Aruma foreland basin. The loading effect of the Semail Ophiolite has a higher impact on the proximal wells with up to 1.8 km (e.g., Aman-1 and Rahmah-1x) of flexural tectonic subsidence against the 600–650 m at the distal offshore wells (e.g., Peter-1, Umbarek-1, and Sharjah-2). The magnitude of the flexure, subsurface geometry, and evolution of the Aruma foreland basin suggests that the basin shape is caused by surface and subsurface ophiolite loading of a lithosphere with an effective elastic thickness, T_e, of 20–25 km (Ali et al., 2013; Ali & Watts, 2009).

Furthermore, the tectonic subsidence curves show another uplift event at ~25–18 Ma followed by an increase in subsidence as is clearly seen in the Aman-1, Tibat-1ST, HD-1, HA-1, Salama-1, Sajaa-1, and Henjam-1 wells (Figures 13d, 13e, 13l, 13m, 13n, 13b, and 13c). For example, the Henjam-1 well drilled along the Hagab thrust shows up to ~1 km of tectonic subsidence during Oligocene–Miocene. The uplift corresponds in time to the collision of the Arabian plate with the Eurasian plate, which started in the late Oligocene with indentation of the Musandam peninsula and initiation of the Hagab thrust (Searle, 1988a, 1988b; Searle et al., 1983). Similar to the Late Cretaceous orogeny, the folds and thrusts of Musandam culmination acted as a load. We therefore attribute the excess subsidence to the development of the Pabdeh foreland basin by flexural loading of the underlying Aruma foreland basin and Arabian plate rifted continental margin. However, the distal wells located away from the load, in offshore Sharjah (Peter-1, Umbarek-1, and Sharjah-2; Figures 13g, 13h, and 13i), did not capture the uplift but showed considerable Oligocene–Miocene subsidence, with 780–980 m of tectonic subsidence (Figures 13g, 13h, and 13i). An additional flexure effect caused by orogenic loading along the Zagros Fold Belt in the north (~200 km) is a possible explanation of such excess subsidence.

The observations of the backstrip curves are in agreement with the seismic interpretation that confirms the Late Cretaceous Aruma foreland basin and the mid-Cenozoic Pabdeh foreland basin in the western Musandam peninsula. Moreover, all the wells drilled in the western Musandam peninsula region show that the heat flow is low, as would be expected for foreland basins. For example, Hagil-1x showed maximum temperature at TD (4,126 m) of 96°C, and Tibat-1ST well displayed a temperature of 107°C at 2,875 m.

7. Conclusions

We draw the following conclusions from this study:

1. Seismic stratigraphy shows that the subsurface architecture of the western side of the Musandam peninsula can be divided into five main sequences: (1) Permian–Cretaceous rifted margin sequence, (2) Upper Cretaceous Aruma foreland basin sequence that evolved in response to the Semail Ophiolite obduction, (2) early–mid-Cenozoic Pabdeh foreland basin sequence that formed by loading of the allochthonous Musandam carbonates associated with the early continent–continent collision of the Arabian plate with the Eurasian plate, (4) late Cenozoic (Fars Group), and (5) a sequence above the late Pliocene unconformity that marks the final continental collision expressed along the Zagros Fold Belt.
2. Seismic profiles and outcrop data captured multiple west-verging and east-dipping thrust faults associated with frontal deformation of the Hagab thrust, which causes repetition of the Mesozoic and early–mid-Cenozoic foreland basin sequences.
3. The Oligocene thrusting of the Musandam peninsula was a thick-skinned event with thrusts cutting both Permian–Mesozoic and pre-Permian basement rocks. The majority of fault tip lines terminate along the base of the Miocene Fars and Mishan Formations below the prominent mid-Miocene unconformity, which marks the timing of the end of the Musandam culmination.
4. Biostratigraphic data from 17 exploration wells suggest that the western Musandam peninsula experienced two rifting events punctuated by periods of slower subsidence or uplift and thermal subsidence. The first rift phase initiated ~260 Ma with rift duration of ~5–7 Myr and a stretching value, β, of 1.09. The second rifting event started ~185 Ma with rift duration of ~10 Myr and β values of 1.08–1.155.
5. The backstrip curves suggest an uplift and the subsequent subsidence that begins ~94 Ma and ~80 Ma, respectively. The uplift and subsidence were attributed to the orogenic loading associated with flexure of the underlying rifted margin, which formed the Aruma foreland basin.
6. The tectonic subsidence curves show another uplift event at ~25–18 Ma followed by an increase in subsidence. The uplift is attributed to the culmination of the Musandam peninsula as a result of the collision between the Arabian and Eurasian plates. The excess subsidence was attributed to the development of the Pabdeh foreland basin by flexural loading of the Musandam peninsula.

Acknowledgments
We are grateful to the Petroleum Institute for sponsoring this project (project LTR14011). We wish to thank DNO and the Government of Ras Al Khaimah for permission to publish the seismic data and some of the wells used in this study. The data used will be made available in the Petroleum Institute's repository site. We thank Douglas Paton, Dominique Frizon de Lamotte, and two anonymous referees for their helpful comments on an earlier version of the paper.

References

Al-Husseini, M. I. (2000). Origin of the Arabian Plate structures; Amar collision and Najd Rift. *GeoArabia*, *5*(4), 527–542.
Al-Husseini, M. I. (2004). Pre-Unayzah unconformity, Saudi Arabia. Carboniferous, Permian and Early Triassic Arabian stratigraphy. *GeoArabia Special Publication*, *3*, 15–59.

Ali, M. Y., & Watts, A. B. (2009). Subsidence history, gravity anomalies and flexure of the United Arab Emirates (UAE) foreland basin. *GeoArabia*, *14*(2), 17–44.
Ali, M. Y., Sirat, M., & Small, J. (2008). Geophysical investigation of Al Jaww Plain, eastern Abu Dhabi: Implications for structure and evolution of the frontal fold belts of the Oman Mountains. *GeoArabia*, *13*(2), 91–118.
Ali, M. Y., Watts, A. B., & Searle, M. P. (2013). Seismic stratigraphy and subsidence history of the United Arab Emirates (UAE) rifted margin and overlying foreland basins. In K. A. Hosani, F. Roure, R. Ellison, & S. Lokier (Eds.), *Lithosphere dynamics and sedimentary basins: The Arabian plate and analogues* (pp. 127–143). Berlin Heidelberg: Springer-Verlag.
Ali, M. Y., Watts, A. B., & Farid, A. (2014). Gravity anomalies of the United Arab Emirates: Implications for basement structures and infra-Cambrian salt distribution. *Geo Arabia*, *19*(1), 85–112.
Ali, M. Y., Fairhead, J. D., Green, C. M., & Noufal, A. (2017). Basement structure of the United Arab Emirates derived from an analysis of regional gravity and aeromagnetic database. *Tectonophysics*, *712*, 503–522.
Al-Laboun, A. A. (1987). Unayzah Formation: A new Permian–Carboniferous unit in Saudi Arabia. *American Association of Petroleum Geologists Bulletin*, *71*, 29–38.
Alsharhan, A. S. (1989). Petroleum geology of the United Arab Emirates. *Journal of Petroleum Geology*, *12*(3), 253–288.
Al-Suwaidi, A. H., Steuber, T., & Suarez, M. B. (2016). The Triassic–Jurassic boundary event from an equatorial carbonate platform (Ghalilah Formation, United Arab Emirates). *Journal of the Geological Society*, *173*(6), 949–953.
Bassin, C., Laske, G., & Masters, G. (2000). The current limits of resolution for surface wave tomography in North America. *Eos, Transactions of the American Geophysical Union*, *81*, F897.
Bechennec, F., Le Metour, J., Rabu, D., Bourdillon-de-Grissac, C., de Wever, P., Beurrier, M., & Villey, M. (1990). The Hawasina Nappes; stratigraphy, palaeogeography and structural evolution of a fragment of the South-Tethyan passive continental margin. *Geological Society Special Publication*, *49*, 213–223.
Cochran, J. R. (1981). Simple models of diffuse extension and the pre-seafloor spreading development of the continental margin of the northeastern Gulf of Aden. *Oceanologica Acta*, *4*, 155–165.
Ellouz, N., Patriat, M., Gaulier, J.-M., Bouatmani, R., & Sabounji, S. (2003). From rifting to Alpine inversion; Mesozoic and Cenozoic subsidence history of some Moroccan basins. *Sedimentary Geology*, *156*(1–4), 185–212.
Faqira, M., Rademakers, M., & Afifi, A. M. (2009). New insights into the Hercynian Orogeny, and their implications for the Paleozoic hydrocarbon system in the Arabian Plate. *GeoArabia*, *14*(3), 199–228.
Forbes, G. A., Jansen, H. S. M., & Schreurs, J. (2010). *Lexicon of Oman subsurface stratigraphy: Reference guide to the stratigraphy of Oman's hydrocarbon basins* (p. 371). Bahrain: Gulf PetroLink.
Frizon de Lamotte, D., Tavakoli-Shirazi, S., Leturmy, P., Averbuch, O., Mouchot, N., Raulin, C., … Ringenbach, J.-C. (2013). Evidence for Late Devonian vertical movements and extensional deformation in northern Africa and Arabia: Integration in the geodynamics of the Devonian world. *Tectonics*, *32*, 107–122. https://doi.org/10.1002/tect.20007
Glennie, K. W., Boeuf, M. G., Hughes-Clarke, M. H. W., Moody-Stuart, M., Pilaar, W. F., & Reinhardt, B. M. (1974). *Geology of the Oman mountains* (p. 423). Amsterdam: Verhandelingen van het Koninklijk Nederlands Geologisch Mijnbouwkundidg Genootschap.
Gradstein, F. M., Ogg, J. G., & Schmitz, M. D. (2012). *The geologic time scale 2012* (p. 1176). Amsterdam: Elsevier.
Hanne, D., White, N., & Lonergan, L. (2003). Subsidence analyses from the Betic Cordillera, Southeast Spain. *Basin Research*, *15*(1), 1–21.
Haq, B. U., & Al-Qahtani, A. M. (2005). Phanerozoic cycles of sea-level change on the Arabian Platform. *GeoArabia*, *10*(2), 127–160.
Haq, B. U., & Schutter, S. R. (2008). A chronology of Paleozoic sea-level changes. *Science*, *322*(5898), 64–68.
Heller, P. L. (1983). *Sedimentary response to Eocene tectonic rotation in Western Oregon (Washington, Pacific Northwest, Petrology)*. Tucson, AZ: The University of Arizona.
Hudson, R. G. S., McGugan, A., & Morton, D. M. (1954). The structure of the Jebel Hagab area, Trucial Oman. *Quarterly Journal of the Geological Society*, *110*(1–4), 121–152.
Husseini, M. I. (1992). Upper Palaeozoic tectono-sedimentary evolution of the Arabian and adjoining plates. *Journal of the Geological Society*, *149*(3), 419–429.
Indago-Petroleum (2006). HAGIL-1 geological completion report (unpublished)*Rep*.
Jahani, S., Callot, J. P., Letouzey, J., & Lamotte, D. F. (2009). The eastern termination of the Zagros fold-and-thrust belt, Iran: Structures, evolution, and relationships between salt plugs, folding, and faulting. *Tectonics*, *28*, TC6004. https://doi.org/10.1029/2008TC002418
Johnson, J. (1985). *Well completion report, Rahmah-1xRep* (pp. 1–17). Ras Al Al Khaimah: Gulf Oil Ras Al Khaimah Ltd.
Johnson, C. (2008). Phanerozoic plate reconstructions of the Middle East: Insights into the context of Arabian tectonics and sedimentation, paper presented at Abu Dhabi International Petroleum Exhibiion and Conference, Society of Petroleum Engineers, Abu Dhabi, UAE, 2008/1/1/.
Johnson, J., & Frost, S. H. (1981). *Well completion report, Jiri-1xRep* (pp. 1–42). Ras Al Khaimah: Gulf Oil Ras Al Khaimah Ltd.
Konert, G., Afifi, A. M., Al-Hajri, S. I. A., & Droste, H. J. (2001). Paleozoic stratigraphy and hydrocarbon habitat of the Arabian Plate. *GeoArabia*, *6*(3), 407–442.
Koop, W. J., & Stonely, R. (1982). Subsidence history of the Middle East Zagros Basin, Permian to Recent. *Philosophical Transactions of the Royal Society of London*, *A302*, 149–168.
Le Nindre, Y.-M., Vaslet, D., Le Metour, J., Bertrand, J., & Halawani, M. (2003). Subsidence modeling of the Arabian platform from Permian to Paleogene outcrops. *Sedimentary Geology*, *156*(1–4), 263–285.
Maurer, F., Rettori, R., & Martini, R. (2008). Triassic stratigraphy, facies and evolution of the Arabian shelf in the northern United Arab Emirates. *International Journal of Earth Sciences*, *97*(4), 765–784.
Michaelis, P. L., & Pauken, R. J. (1990). Seismic interpretation of the structure and stratigraphy of the Strait of Hormuz. *Geological Society of London, Special Publication*, *49*, 387–395.
Miller, K. G., Kominz, M. A., Browning, J. V., Wright, J. D., Mountain, G. S., Katz, M. E., … Pekar, S. F. (2005). The Phanerozoic record of global sea-level change. *Science*, *310*(1293).
Patriat, M., Ellouz, N., Dey, Z., Gaulier, J.-M., & Ben Kilani, H. (2003). The Hammamet, Gabes and Chotts basins (Tunisia); A review of the subsidence history. *Sedimentary Geology*, *156*(1–4), 241–262.
Patton, T. L., & O'Connor, S. J. (1988). Cretaceous flexural history of northern Oman mountain foredeep, United Arab Emirates. *American Association of Petroleum Geologists Bulletin*, *72*(7), 797–809.
Philips, T. (2013). Subsidence history and structure of UAE foreland basin and underlying passive margin sequences, Oxford.
Raiga-Clemenceau, J., Martin, J. P., & Nicoletis, S. (1998). The concept of acoustic formation factor for more accurate porosity determination from sonic transit data. *The Log Analyst*, *29*, 54–60.

Reuning, L., Schoenherr, J. A., Heimann, J. L., Urai, R., Littke, P. A., & Rawahi, Z. (2009). Constraints on the diagenesis, stratigraphy and internal dynamics of the surface-piercing salt domes in the Ghaba Salt Basin (Oman): A comparison to the Ara Group in the South Oman Salt Basin. *GeoArabia*, *14*(3), 83–120.

Ricateau, R., & Riche, P. H. (1980). Geology of the Musandam Peninsula (Sultanate of Oman) and its surroundings. *Journal of Petroleum Geology*, *3*(2), 139–152.

Robertson, A. H. F. (1986). Geochemical evidence for the origin of Late Triassic melange units in the Oman mountains as a small ocean basin formed by continental rifting. *Earth and Planetary Science Letters*, *77*(3–4), 318–332.

Robertson, A. H. F., & Searle, M. P. (1990). The northern Oman Tethyan continental margin; stratigraphy, structure, concepts and controversies. *Geological Society Special Publication*, *49*, 3–25.

Ruban, D. A., Al-Husseini, M. I., & Iwasaki, Y. (2007). Review of Middle East Paleozoic plate tectonics. *Geoarabia*, *12*(3), 35–55.

Schneider, F., Potdevin, J. L., Wolf, S., & Faille, I. (1996). Mechanical and chemical compaction model for sedimentary basin simulators. *Tectonophysics*, *263*(1), 307–317.

Searle, M. P. (1988a). Thrust tectonics of the Dibba Zone and the structural evolution of the Arabian continental margin along the Musandam Mountains (Oman and United Arab Emirates). *Journal of the Geological Society of London*, *145*(1), 43–53.

Searle, M. P. (1988b). Structure of the Musandam culmination (Sultanate of Oman and United Arab Emirates) and the Straits of Hormuz syntaxis. *Journal of the Geological Society*, *145*(5), 831–845.

Searle, M. P. (2007). Structural geometry, style and timing of deformation in the Hawasina window, Al Jabal al Akhdar and Saih Hatat culminations, Oman mountains. *Geo Arabia*, *12*, 99–130.

Searle, M. P., & Ali, M. Y. (2009). Structural and tectonic evolution of the Jabal Sumeini–Al Ain–Buraimi region, northern Oman and eastern United Arab Emirates. *GeoArabia*, *14*(1), 115–142.

Searle, M. P., & Malpas, J. (1980). Structure and metamorphism of rocks beneath the Semail ophiolite of Oman and their significance in ophiolite obduction. *Transactions of the Royal Society of Edinburgh: Earth Sciences*, *71*(4), 247–262.

Searle, M. P., James, N. P., Calon, T. J., & Smewing, J. D. (1983). Sedimentological and structural evolution of the Arabian continental margin in the Musandam Mountains and Dibba Zone, United Arab Emirates. *Geological Society of America Bulletin*, *94*(12), 1381–1400.

Searle, M. P., Cooper, D. J. W., Watts, K. F., Robertson, A. H. F., & Ries, A. C. (1990). Structure of the Jebel Sumeini-Jebel Ghawil area, northern Oman. *Geological Society Special Publication*, *49*, 361–374.

Searle, M. P., Cherry, A. G., Ali, M. Y., & Cooper, J. W. (2014). Tectonics of the Musandam Peninsula and northern Oman Mountains: From ophiolite obduction to continental collision. *GeoArabia*, *19*(2), 135–174.

Searle, M. P., Waters, D. J., Garber, J. M., Rioux, M., Cherry, A. G., & Ambrose, T. K. (2015). Structure and metamorphism beneath the obducting Oman ophiolite: Evidence from the Bani Hamid granulites, northern Oman mountains. *Geosphere*, *11*(6), 1812–1836.

Sharland, P. R., Archer, R., Casey, D. M., Davies, R. B., Hall, S. H., Heward, A. P., … Simmons, M. D. (2001). *Arabian plate sequence stratigraphy*, (pp. 1–371). Manama: Gulf Petro-Link.

Stampfli, G., Marcoux, J., & Baud, A. (1991). Tethyan margins in space and time. *Palaeogeography, Palaeoclimatology, Palaeoecology*, *87*(1), 373–409.

Stampfli, G. M., Mosar, J., Favre, P., Pillevuit, A., & Vannay, J.-C. (2001). Permo-Mesozoic evolution of the western Tethys realm: the Neo-Tethys East Mediterranean basin connection. In P. A. Ziegler, et al. (Eds.), *Peri-Tethys Memoir 6: Peri-Tethyan rift/wrench basins and passive margins* (pp. 51–108). Paris: Mémoires du Muséum National d Histoire Naturelle de Paris.

Steckler, M. S., & Watts, A. B. (1978). Subsidence of the Atlantic-type continental margin off New York. *Earth and Planetary Science Letters*, *41*, 1–13.

Stern, R. J., Ren, M., Ali, K., Förster, H.-J., Al Safarjalani, A., Nasir, S., … Romer, R. L. (2014). Early Carboniferous (~357 Ma) crust beneath northern Arabia: Tales from Tell Thannoun (southern Syria). *Earth and Planetary Science Letters*, *393*, 83–93.

Stewart, S. A. (2016). Structural geology of the Rub' Al-Khali Basin, Saudi Arabia. *Tectonics*, *35*, 2417–2438. https://doi.org/10.1002/2016TC004212

Stewart, S. A., Reid, C. T., Hooker, N. P., & Kharouf, O. W. (2016). Mesozoic siliciclastic reservoirs and petroleum system in the Rub' Al-Khali basin, Saudi Arabia. *AAPG Bulletin*, *100*(5), 819–841.

Styles, M. T., Ellison, R. A., Arkley, S. L. B., Crowley, Q., Farrant, A., Goodenough, K. M., … Thomas, R. J. (2006). *The geology and geophysics of the United Arab Emirates* (pp. 1–351). Ministry of Energy, United Arab Emirates, Keyworth: British Geological Survey.

Tarapoanca, M., Andriessen, P., Broto, K., Chérel, L., Ellouz-Zimmermann, N., Faure, J.-L., … Roure, F. (2010). Forward kinematic modelling of a regional transect in the Northern Emirates using geological and apatite fission track age constraints on paleo-burial history. *Arabian Journal of Geosciences*, *3*(4), 395–411.

Tavakoli-Shirazi, S., Frizon de Lamotte, D., Wrobel-Daveau, J.-C., & Ringenbach, J.-C. (2013). Pre-Permian uplift and diffuse extensional deformation in the High Zagros Belt (Iran): Integration in the geodynamic evolution of the Arabian plate. *Arabian Journal of Geosciences*, *6*(7), 2329–2342.

Warburton, J., Burnhill, T. J., Graham, R. H., & Isaac, K. P. (1990). The evolution of the Oman mountains foreland basin. *Geological Society, London, Special Publications*, *49*(1), 419–427.

Watts, A. B., & Ryan, W. B. F. (1976). Flexure of the lithosphere and continental margin basins. *Tectonophysics*, *36*, 24–44.

Watts, A. B., & Steckler, M. S. (1979). Subsidence and eustasy at the margin of eastern North America. *American Geophysical Union*, *3*, 218–234.

Wyllie, M. R. J., Gregory, A. R., & Gardner, L. W. (1956). Elastic wave velocities in heterogeneous and porous media. *Geophysics*, *21*(1), 41–70.

Ziegler, M. A. (2001). Late Permian to Holocene paleofacies evolution of the Arabian Plate and its hydrocarbon occurrences. *GeoArabia*, *6*(3), 445–504.